water

MDPI

Review

# N–$TiO_2$ Photocatalysts: A Review of Their Characteristics and Capacity for Emerging Contaminants Removal

**João Gomes *, João Lincho, Eva Domingues, Rosa M. Quinta-Ferreira and Rui C. Martins**

CIEPQPF—Chemical Engineering Processes and Forest Products Research Center, Department of Chemical Engineering, Faculty of Sciences and Technology, University of Coimbra, Rua Sílvio Lima, 3030-790 Coimbra, Portugal; uc2015249034@student.uc.pt (J.L.); evadomingues@eq.uc.pt (E.D.); rosaqf@eq.uc.pt (R.M.Q.-F.); martins@eq.uc.pt (R.C.M.)

* Correspondence: jgomes@eq.uc.pt; Tel.:+35-1239798723

Received: 2 January 2019; Accepted: 15 February 2019; Published: 21 February 2019

**Abstract:** Titanium dioxide is the most used photocatalyst in wastewater treatment; its semiconductor capacity allows the indirect production of reactive oxidative species. The main drawback of the application of $TiO_2$ is related to its high band-gap energy. The nonmetal that is most often used as the doping element is nitrogen, which is due to its capacity to reduce the band-gap energy at low preparation costs. There are multiple and assorted methods of preparation. The main advantages and disadvantages of a wide range of preparation methods were discussed in this paper. Different sources of N were also analyzed, and their individual impact on the characteristics of N–$TiO_2$ was assessed. The core of this paper was focused on the large spectrum of analytical techniques to detect modifications in the $TiO_2$ structure from the incorporation of N. The effect of N–$TiO_2$ co-doping was also analyzed, as well as the main characteristics that are relevant to the performance of the catalyst, such as its particle size, surface area, quantum size effect, crystalline phases, and the hydrophilicity of the catalyst surface. Powder is the most used form of N–$TiO_2$, but the economic benefits and applications involving continuous reactors were also analyzed with supported N–$TiO_2$. Moreover, the degradation of contaminants emerging from water and wastewater using N–$TiO_2$ and co-doped $TiO_2$ was also discussed.

**Keywords:** N–$TiO_2$; preparation methods; co-doping; emerging contaminants; sunlight degradation; catalysts characterization techniques; photocatalytic oxidation

## 1. Introduction

Titanium dioxide is the most widely used photocatalyst material due to its semiconductor characteristics, which make it a remarkable option for photocatalysis applications involving solar or other sources of radiation [1–3]. Along time, several uses were found for titanium dioxide such as hydrogen production, photovoltaic cells, self-cleaning surfaces, air purification, anti-fogging surfaces, adjuvant on heat transfer and dissipation, anticorrosion applications, environmentally-friendly surface treatment, photocatalytic lithography, photochromism, etc. [4–7]. However, the application of this material as the catalyst for wastewater treatment through heterogeneous photocatalysis gained force in the last years [7–10].

Water scarcity is one of the major global problems of this century. The exponential growth of the world population and global warming are the main reasons for this problem. Conventional wastewater treatments alone are not suitable for water reclamation, since the presence of chemical and biological emerging contaminants that are refractory to these methodologies can be detected in the effluents of wastewater treatment plants as well as at the rivers and lakes where this treated water is disposed [11].

In a preferred scenario, the future of water supply must go through water reuse from wastewater treatment plants. However, focus is needed on new treatment technologies involving low investment and operational costs to attract stakeholders. The scientific community is working on the development of new technologies for this purpose. The use of $TiO_2$ is an interesting alternative in these studies, since there is the possibility of using it with sunlight radiation to promote the removal of pollutants from water, which would reduce water treatment costs.

Titanium dioxide is an easy-to-handle material that is very chemically stable when compared to other catalysts, and can be found at low cost. Titanium dioxide can present three different phases of polymorphs: anatase, rutile, and brookite [12]. Anatase and rutile are the most commonly studied phases in the photocatalytic experiments, since anatase is the most photocatalytically active, whereas rutile is thermodynamically more stable [12,13]. Regarding brookite, few studies exist related to its surface structure characterization [12].

Titanium dioxide is a semiconductor. Thus, a suitable source of energy can promote the transfer of electrons from the valence band to the conduction band. The energy needed to promote the photogeneration of electron–holes pairs is usually called a band gap. If this band gap is small enough, solar energy can be used as the primary source of radiation to activate this kind of catalyst. Reversely, if the band gap is high, ultra-violet (UV) radiation shall be needed. In terms of the process, when this band gap is broken or disrupted, leading to the previously described electron transfer, the titanium dioxide can promote the degradation of contaminants from the wastewater [1]. The photogenerated electron–hole pair will allow the oxidation of water and/or organic matter as well as the reduction of oxygen and other reactive oxidative species, leading to radical moieties that are able to oxidize pollutants at the liquid bulk [2,3]. For instance, in real wastewater, some other species are present (such as $Cl^-$, $HCO_3^-$, $CO_3^{2-}$, and $SO_4^{2-}$), which can be reduced, producing radicals that can help with the degradation process of organic contaminants [14].

The typical band-gap energy of titanium dioxide is between 3–3.2 eV. Thus, UVA radiation (wavelength <400 nm) is needed for its activation. Sunlight radiation just comprises 4–5% of UVA radiation. This means that low performance is expected when natural light is applied. Therefore, to take advantage of the remaining spectrum of sunlight radiation, the visible region, the $TiO_2$ band gap must be reduced. This is usually achieved by using a suitable dopant. Doping appears as a good alternative for changing the activity of $TiO_2$ catalysts through the optoelectrical modification of this material by the introduction of dopants with different energy levels between the conduction and valence band [15]. The applied dopants can be metals, such as noble and transition metals, or nonmetals (N, B, S, F, and C). The noble metals (such as Ag, Au, Pd, and Pt) present some advantages such as the possibility to absorb the visible light due to the surface plasmon resonance [16–18], but the high cost associated with these materials should be considered a disadvantage. The transition metals can also enhance their photocatalytic activity. However, their leaching behavior leads to the fast deactivation of the catalyst and constitutes a second source of pollution, requiring the removal of dissolved metals from treated water [3]. Therefore, nonmetals present some advantages compared to the metal dopants. Besides the effective activation of $TiO_2$ in the visible spectrum of sunlight due to the narrowing of the band gap that allows avoiding the recombination phenomenon, the low cost and environmentally-friendly character of this material appear as tempting features [19]. As nonmetal doping elements, some anionic species such as nitrogen, carbon, sulfur, and boron have been studied due to the beneficial advantages of substituting oxygen in a $TiO_2$ lattice and given activity to these catalysts at visible light radiation, maintaining its maximum efficiency [15,20,21]. Among the above-mentioned nonmetals, the most suitable and commonly used is nitrogen. This element can introduce few states at the valence band edge, tuning the optical band gap and acting as superficial donors [15,22]. Moreover, N instead of O in the $TiO_2$ lattice allows the band gap to narrow due to the 2p states of the N atom mixed with O 2p states [23,24]. In fact, it was proved that for both the anatase and rutile phases of $TiO_2$, the N 2p states were located just above the top of the O 2p valence band, which means a red shift of the absorption band edge to the visible region [23]. Therefore, it indicates that nitrogen is the best nonmetal dopant

to $TiO_2$, improving the photocatalytic activity at the visible light radiation, which means a low-cost energy source for the degradation of contaminants.

In this context, N–$TiO_2$ catalysts are interesting in this field, and lots of information about them can be found in the literature. However, data about the main changes provided by nitrogen doping or co-doping in $TiO_2$ is not well established and defined. In fact, to the best of our knowledge, there is no overview on the subject. In the present study, the main objective is to critically overview the information about N doping and co-doping changes in the characterization analysis of the typical catalysts. Then, we can understand the advantages of using these catalysts in advanced oxidation technologies for wastewater treatment, especially in what regards emerging contaminants removal. Another feature that will be analyzed is the advantage between using powder and supported $TiO_2$ for wastewater treatment. Finally, future perspectives regarding this kind of catalyst will be discussed considering the wastewater treatment applications.

## 2. Effect of the Catalyst Preparation Method

A wide range of preparation methods for doped forms of titanium dioxide can be found in the literature (Table 1). The most common are ion implantation [25], sintering at high temperature [20,26,27], plasma processes [28], the hydrothermal method [29–32], the oxidation of titanium nitride [33–35], the sol–gel method [15,21,36,37] hydrolysis [4,8,38], chemical modifications [39], and low-temperature nitridization [40]. The effect of the preparation methods on the N–$TiO_2$ activity for green energy applications was revised by Devi and Kavitha [41]. Thus, this section will focus on the effect of the catalyst preparation procedure, especially for water/wastewater treatment through the photocatalytic oxidation of contaminants.

Ion implantation consists of ion bombardment on the $TiO_2$ powder or film. Therefore, a special implanter will be needed which, besides the energy required for ion bombardment, can represent a negative impact regarding the cost of the catalyst production. Ghicov et al. [25] prepared N–$TiO_2$ nanotubes using an ion bombardment of N at the nominal dose of $1 \times 10^{16}$ ions/cm$^2$ with an accelerating energy of 60 keV. The $TiO_2$ nanotubes were previously prepared by anodization. In this study, the ion implantation promotes a significant band gap decrease from 3.15 to 2.20 eV, but during the implantation, anatase changes to amorphous phase. Thus, a calcination step was then required (450 °C for three hours) to convert it again into anatase [25].

The sintering of $TiO_2$ powders at high temperatures in the presence of $N_2$ and $NH_3$ gas is the conventional method to produce N–$TiO_2$. Nevertheless, the amount of nitrogen that can be doped with this method is limited [20]. Besides, the operational conditions imply more restrictive equipment [20,26]. Asahi et al. [26] produced N–$TiO_2$ by sputtering the $TiO_2$ with an $N_2$ (40%)/Ar gas mixture annealed at 550 °C over four hours, and as comparison, pure $TiO_2$ was obtained through the sputtering with an $O_2$ (20%)/Ar gas mixture at the same conditions. The high temperatures promoted agglomeration and pore structure collapse, leading to the reduction of the active surface area. This can decrease the performance when photocatalysis is considered. Another example of sintering at high temperatures is the annealing method [27]. In this method, the titanium and nitrogen precursor solids are mixed together, heated, and calcinated at the same time for three hours at 350 °C. The heat treatment can promote a change in the physical and chemical properties of the crystal, allowing the incorporation of nitrogen into a $TiO_2$ lattice. This method allows the production of N–$TiO_2$ in a single step, and different amounts of nitrogen can be used. However, it is important to evaluate the yield of the process regarding the level of nitrogen incorporation. On the other hand, the use of $NH_3$ may represent an environmental issue due to air pollution through its erosive and toxic characteristics [4].

In the same way, the plasma process involves a high consumption of energy in the plasma reactor and during the annealing of the material at high temperatures [28]. Chen et al. [28] mixed titanium tetraisopropoxide, water vapor, and $N_2$ stream before feeding it into a plasma reactor. This plasma reactor has two electrodes and an electrical field of 9.6 kV/cm at atmospheric pressure, which represents a power consumption of about nine W [28]. Afterwards, the resulting powder from the plasma process

was annealed at 500 °C for three hours to promote the formation of the anatase phase [28]. This process needed some special conditions such as a gas stream and a reactor with the suitable characteristics, which can represent an important budget in terms of implantation costs. On the other hand, the amount of catalyst produced is very dependent upon the reactor size.

The hydrothermal method implies the utilization of high temperature and pressure conditions, requiring suitable equipment for these kinds of reactions. This process was truly believed as being the best over other methods, since high amounts of nitrogen can be doped in $TiO_2$ [30]. With up to 5% mol of nitrogen incorporated, in the past, it was believed that other methods would not be able to dope such amounts of nitrogen in a $TiO_2$ lattice [20,29]. However, Burda et al. [29], using a direct amination of the titania particles were able to dope 8% mol of nitrogen by reducing the doping reaction speed. Later, Peng et al. [30] produced N–$TiO_2$ via the hydrothermal method using triethanolamine as the N precursor and Degussa P25 as the $TiO_2$ source. The reaction inside an autoclave at 140 °C was run over 24 h. The catalyst did not suffer significant modifications in terms of the constitution of phases compared to the typical ones of P25 (80% anatase and 20% rutile). This study proved that the doping can be up to 21% mol in N, corresponding to a Ti:N:O ratio of 1:0.86:2.25, respectively. The new molecular form produced by Peng et al. [30], $TiO_{2.25}N_{0.86}$, disagreed with the other proposed $N_xTiO_{2-x}$ structures [20]. Therefore, it was concluded that the hydrothermal method does not just substitute oxygen atoms by nitrogen, but it can also substitute titanium by nitrogen due to the high pressure applied with this methodology [30].

As previously described, the predominant phases of $TiO_2$ are anatase and rutile. Normally, the produced titania catalysts are mainly constituted by the anatase phase. Hu et al. [31] synthetized N–$TiO_2$ using titanium tetrachloride and urea via hydrothermal conditions at 105 °C over six hours. After this process, the ratio between the anatase and rutile phases was about 50:50. However, just 0.7% mol of nitrogen in the titanium dioxide was obtained. The authors verified impurity levels above the valence band, which allowed the usage of visible light irradiation [31]. In order to reduce the high pressure and temperature costs related with the conditions of the typical hydrothermal method, the UV-assisted thermal method was proposed as a cost-effective alternative [27]. In this method, the UV-C light was applied to assist the synthesis of the photocatalyst. For this, an ordinary glassware was used with a condenser coupled at normal pressure and low temperature. However, after that, the catalyst needs to be calcinated over three hours at 350 °C. Nasirian and Mehvrar [27] noted that this method produces a N–$TiO_2$ catalyst with a large surface area and high photocatalytic activity. Parallelly, alternative sources of energy can be used for the preparation of catalysts, such as a microwave. This application requires a special reactor that can be suitable to work inside of a microwave generator [27,42]. One of the main problems of this method is the high investment cost with the microwave reactor and the reduced amount of catalyst that can be prepared. These parameters are dependent on the capacity of the microwave reactor. However, the time of reaction will be reduced compared to typical hydrothermal methods [27].

Another perspective of the application of the hydrothermal method is the production of hollow-structured spheres in one step [32]. The presence of a chelating agent to give a microsphere structure can be advantageous in terms of the photocatalytic activity, since the decomposition of rhodamine-B was better with those materials than with P25 powder under sunlight radiation [32]. These preparation method conditions allowed obtaining mainly the anatase phase, as was confirmed from N–$TiO_2$ X-Ray Diffraction (XRD) analysis [32]. Comparing to the previous study, Li et al. [32] used a higher temperature for a longer time, which implies higher costs of production. However, compared to other methods such as sol–gel, this preparation does not need the calcination step.

Looking for the phase transformation during the catalysts' preparation, one that is the responsible for the presence of anatase and rutile in the final material can be the type of titanium precursor [30,31].

The oxidation of titanium nitride (TiN) at hydrothermal conditions can represent a substantial investment cost, since it couples the hydrothermal process with the oxidation under ultrasound energy. Zhou et al. [35] produced N–$TiO_2$ using TiN as a precursor and different amounts of hydrogen

peroxide (1 wt %, 2.5 wt %, 5 wt %, 7.5 wt %, and 10 wt %) as oxidant. For this, TiN was dispersed into a $H_2O_2$ solution and mixed using ultrasonification at 700 W over 10 min. After two hours of stirring, the white solid was transferred to a Teflon-lined autoclave over 24 h at 170 °C [35]. After the hydrothermal step, the powder was washed and dried in air over 24 h at 110 °C [35]. The increase in the amount of the $H_2O_2$ solution promoted a decrease in the N content in the catalyst. It was concluded that the incorporation of N occurs by substitution and NO chemisorption at the catalyst surface. However, this process presents high-energy consumption to achieve a photoactive N–$TiO_2$. Zhu et al. [34] prepared a nitrogen-doped titanium dioxide thin film through the oxidation of sputtered TiN. The amount of nitrogen doped onto thin films was easily controlled by changing the ratio of $N_2$ on the gas mixture that was used for the magnetron-sputtering process with a reactive direct current [34].

The sol–gel method for doped and undoped titania catalysts is the most used approach, due to the simplicity of the process. However, different types of sol–gel can be applied with wide changes regarding the method of application [42]. One of the major advantages is the use of low temperature, allowing a reduction on the production costs. Moreover, it can be done without any special equipment [15,43,44]. In this method, the conditions of preparation can be widely different, so we will focus on a few to describe it.

Barkul et al. [15] produced N–$TiO_2$ from titanium tert-butoxide and urea. After initial preparation of the titanium solution, urea was added at different loadings, and the pH was adjusted to 10 with ammonia. The obtained solution was stirred over three hours at 60 °C, and then was cooled. The resulting precipitate was dispersed in distilled water and stirred again under the same conditions. After that, the final solution was dried at 110 °C and calcinated at 400 °C over five hours [15]. This method presents a low aging time, but a solution to correct the pH is required. Besides, the calcination step must be a little bit longer. Sun et al. [6] produced N–$TiO_2$ from tetrabutyl titanate and urea using the sol–gel method with 24 h of aging at room temperature; then, it was dried at 70 °C.

A study that analyzes N–F-$TiO_2$ preparation by the sol–gel method concluded that the preparation conditions lead to changes in the material characteristics such as those that concern the crystallinity, size, dispersion and band gap. Thus, this will influence the material efficiency regarding photocatalytic degradation [45].

As previously described, the limiting step of the sol–gel process is the time needed to promote the aging of the catalyst. This step can usually go from eight to 48 h. Therefore, ultrasounds can be considered a suitable technology, as they are easy to operate and environmentally friendly, which will allow the reduction of the synthesis time [19,44]. However, compared to some sol–gel methods, the use of ultrasounds can present higher energy costs [19,44]. Ramandi et al. [19] produced N–$TiO_2$ from titanium butoxide and urea using ultrasound energy (20 kHz). The sonication time in a Rosset cell totaled 15 min at 25 °C. After that, the sonicated solution was placed aside to promote the formation of gel. At the end of the process, after the gel drying, the catalyst was calcinated with different temperatures [19]. On the other hand, Lee et al. [44] produced N–$TiO_2$ from titanium butoxide and urea using a modified sol–gel method with ultrasound irradiation just for the doping step. Firstly, $TiO_2$ powder was obtained after six hours of aging, and then, ultrasound energy (20 kHz) was applied for 40 min. This method allows obtaining N–$TiO_2$ without a calcination step [44].

Hydrolysis is comparable to sol–gel; the main difference is the absence of an aging step. In the hydrolysis method, the powder is obtained instantaneously at low temperatures. Normally, the solution was stirred for 30 min [21]. Sacco et al. [38] prepared different aqueous solutions of ammonia to add on the titanium tetraisopropoxide at 0 °C, and the solution was maintained under stirring until the formation of a white precipitate. This precipitate is washed, centrifuged, and dried before calcination for 30 min at 450 °C [38]. Rizzo et al. [8] prepared N–$TiO_2$ by the hydrolysis method and different calcination times (10 min, 20 min, 30 min, and 40 min) at 450 °C using titanium tetraisopropoxide and ammonia solution (30 wt %) as titanium and ammonia sources, respectively. After characterization and degradation experiments, it was concluded that the most active and suitable catalyst was the one prepared using a calcination temperature of 450 °C over 30 min [8]. Yuan et al. [4],

instead of using low temperature, added ammonia to the colloid solution obtained from the hydrolysis of $TiCl_4$, where $OH^-$ neutralized the $H^+$ that was provided from water, leading to the precipitation of $TiO_2$. However, the N present in the ammonia did not work as the N precursor. To promote the doping process, those authors added urea in agate mortar a few minutes after the centrifugal step [4].

Chemical modifications are based on the hydrolysis process, but with some modifications, since instead of working at low temperatures [8,38], it works at low pressure [39]. Nosaka et al. [39] used as N precursors urea, guanidine hydrochloride, and guanidine carbonate on the aqueous form with different $TiO_2$ powder sources. The two precursors were mixed at room temperature and were kept in dark conditions for one day. Afterwards, the mixture was dried at vacuum conditions until obtaining a white powder. The powder was then calcinated at different temperatures (350 °C, 450 °C, and 550 °C) during the period of 30 min, one hour, and five hours. After that, the calcinated powder was washed and dried under reduced pressure [39].

In the same way, the low-temperature nitridization method is based on the incorporation of N into the $TiO_2$ lattice after hydrolysis during the crystallization step, and the peptization time can have an important role on the content of the different phases. Hu et al. [40] used the low-temperature nitridization method using triethylamine as the nitrogen source and tetrabutyltitanate dissolved in ethanol as the titanium precursor. These precursors were stirred at room temperature for 24 h, and the pH value was 12. At those conditions, condensation and crystallization occurred. Then, different amounts of nitric acid (0.1 M, 0.5 M, and 1 M) were added into the solution and peptization took place at 70 °C for different periods of time (four hours, eight hours, 20 h, 36 h, and 48 h) for further crystallization. The concentration increase of acid and peptization times enhanced the rutile phase production. The authors noted that the formation of N–Ti-O bonds is related with the occurrence of nitridization before crystallization. The peptization time of 20 h and nitric acid concentration of 0.5 M provided the most active photocatalyst on the methylene blue decolorization using UV radiation or visible light [40].

As it can be seen, the methods of doped catalyst preparation can present some advantages or disadvantages in terms of photoactivity under visible light for the degradation of organic compounds. One of the main conclusions that should be withdrawn from this section is that the temperature during the preparation has real impact in terms of phase development. The catalysts prepared without high temperature or calcination present, in general, anatase as the predominant phase. Exception goes to the materials prepared by the hydrothermal process, since the high pressures can also influence the phase production. Table 1 summarizes some of the pros and cons for each preparation method, as well as the main operating conditions applied in each work for obtaining N–$TiO_2$.

**Table 1.** Advantages and disadvantages of N–$TiO_2$ preparation methods.

| Ref. | Method | Advantages | Disadvantages |
|---|---|---|---|
| [4] | Hydrolysis | -Fast production;<br>-Does not need low temperature; | -Needs to be washed;<br>-Centrifugation step;<br>-Drying at 200 °C;<br>-Calcination step (350–700 °C);<br>-Agate mortar usage to promote the doping; |
| [21] | Hydrolysis | -Fast production;<br>-Diethanolamine allows anatase production;<br>-Band gap decreases from 3.16 to 2.85 eV for diethanolamine. | -Low temperature (4 °C) for 30 min;<br>-Calcination step (800 °C for 30 min).<br>-Triethylamine and urea produced rutile, which decrease the photoactivity;<br>-Drying at 100 °C for 90 min. |
| [8,38] | Hydrolysis | -Fast production;<br>-Anatase production;<br>-Significant reduction of band gap (3.3 to 2.5 eV); | -Low temperature (0 °C);<br>-Needs to be washed;<br>-Centrifugation step;<br>-Calcination step (450 °C for 30 min). |
| [44] | Sol–gel to $TiO_2$ after ultrasound irradiation for doping | -Aging step at room temperature;<br>-Absence calcination step. | -Two steps;<br>-Aging step time (six h); |

**Table 1.** *Cont.*

| Ref. | Method | Advantages | Disadvantages |
|---|---|---|---|
| [44] | Sol–gel to $TiO_2$ after ultrasound irradiation for doping | -Aging step at room temperature;<br>-Absence calcination step. | -Two steps;<br>-Aging step time (six h); |
| [19] | Sol–gel method coupled with ultrasound treatment | -Room temperature can be used;<br>-Low time of aging (15 min);<br>-Reduced production time; | -Rosset cell needed;<br>-Ultrasound energy (20 kHz);<br>-Calcination step (three hours at 300 °C, 400 °C, and 500 °C);<br>-Two hours after sonication to obtain a gel;<br>-Drying step (10 h at 80 °C) |
| [6] | Sol–gel method | -Aging at room temperature;<br>-Low band gap (2.58 eV); | -Aging time (24 h);<br>-Drying step (70 °C);<br>-Calcination step (400 °C, 500 °C, 600 °C, and 700 °C). |
| [15] | Sol–gel method | -Low time of aging (three hours);<br>-High band-gap reduction from 3.21 to 2.34 for the 7% mol of N doping; | -Aging temperature (60 °C);<br>-Needed additional step (stirring three hours at 60 °C);<br>-Calcination step (five hours at 400 °C);<br>-pH correction to basic conditions;<br>-Drying step (110 °C). |
| [39] | Chemical modifications (such as hydrolysis) | -Reduced time of production; | -Two steps of vacuum drying;<br>-Needs to be washed ($H_2SO_4/H_2O$);<br>-Calcination step (30 min, one hour, and five hours at 350 °C, 450 °C, and 550 °C);<br>-High costs with vacuum; |
| [26] | Sintering at high temperatures | -Significant reduction of the band gap | -High-temperature process (550 °C);<br>-Gas streams needed; |
| [30] | Hydrothermal process | -Allows a great amount of N introduction;<br>-21% of N concentration; | -Autoclave;<br>-High pressure and temperatures;<br>-Reaction time (24 h at 140 °C);<br>-Drying step (10 h at 200 °C). |
| [31] | Hydrothermal process | -Reduced time of production;<br>-Low particle size (five nm);<br>-Produced rutile amount without any high temperature treatment; | -Stainless steel autoclave (30 mL);<br>-High pressure and temperatures;<br>-Reaction time (six hours at 105 °C);<br>-Drying step under vacuum conditions;<br>-Calcination step (10 h at 500 °C). |
| [32] | Hydrothermal method | -Does not need a calcination step;<br>-Hollow spheres production; | -Drying step (12 h at 60 °C);<br>- Teflon-lined autoclave (50 mL);<br>-High pressure and temperatures;<br>-Reaction time (eight hours at 180 °C);<br>-Chelating agent (ethylenediaminetetraacetic acid, or EDTA); |
| [28] | Plasma process | | -Plasma reactor;<br>-Calcination at high temperatures;<br>-High voltage for reactor; |
| [25] | Ion implantation | -Reduction of band gap from 3.15 eV to 2.2 eV; | -Ion implanter;<br>-Energy costs;<br>-Calcination step; |
| [35] | Oxidation of titanium nitride | -N-substituitional; | -Hydrothermal step for 24 h at 170 °C;<br>-Presence of hydrogen peroxide;<br>-Ultrasonification energy (700 W);<br>-Need to be washed and dried (24 h at 110 °C) |
| [40] | Low temperature of nitridization | -Different proportions of the rutile and anatase phase;<br>-Absence of calcination step; | -Higher times for peptization (20 h);<br>-Temperature of 70 °C for peptization; |

## 3. Type of Nitrogen Source

The nitrogen source should be selected according to the precursor for titanium dioxide. These precursors can change the catalytic properties and photoactivity of the catalysts [15,21,45]. Also, the method chosen for the production of catalysts is very dependent upon the nitrogen and titanium dioxide precursors. For example, the most common nitrogen precursors for the sol–gel method are ammonia hydroxide, urea, diethanolamine, and triethylamine [21,46]. Ananpattarachai et al. [21] studied three different types of nitrogen precursors for $TiO_2$ doping—urea, diethanolamine, and triethylamine—using the sol–gel method and titanium tetraisopropoxide as the titanium source.

For all the catalysts produced, the incorporation of nitrogen into the $TiO_2$ lattice was interstitial. From the different N precursors studied, the most active under visible light for 2-chlorophenol degradation was diethanolamine. This dopant led to the smallest band gap and the smallest anatase crystal size, which will increase the surface area of the catalyst, and consequently the availability of the active sites [21]. In fact, for the materials prepared using other dopant precursors, the band gap was higher, as well as the crystal size. Moreover, the N–$TiO_2$ that is produced presents some fraction of the rutile phase, which decreases the photocatalytic activity [21]. The use of primary and secondary amines seems to be able to provide a more suitable N–$TiO_2$ due to the structure and the accessibility of nitrogen atoms to react with the titanium precursor [21]. Moreover, triethylamine can prevent the aggregation of N–$TiO_2$ particles, assuring the good dispersibility of the grains [40].

On the other hand, the ammonium hydrogen carbonate can also be used as an N precursor, as described in the work by Mekprasart and Pecharapa [47], where N–$TiO_2$ was produced from ammonium hydrogen carbonate over P25 (Aeroxide) nanopowders with nitrogen doping amounts of 10 wt %, 30 wt %, and 50 wt %. The authors indicate that this precursor is a good option, but also concluded that the crystallite size was reduced compared to P25 due to the presence of hydroxyl carbonate onto the N–$TiO_2$ lattice. Moreover, an absorption spectrum at the UV region instead of the visible region was verified for the highest (50 wt %) and lowest (10 wt %) amount of nitrogen. The authors explained that for 10 wt %, this can be related to the low availability of nitrogen atoms and for 50 wt %, the reason was related to the difficulty of decomposing such a huge amount of precursor to combine with $TiO_2$. Two other reasons—the method selected to produce this catalyst and the precursor used—can support these results, since other precursors with a higher amount of nitrogen promoted significant differences on the absorption spectrum, pushing it to the visible region compared to undoped $TiO_2$ [30,48].

Anther nitrogen source is 1,3-diaminopropane. Nolan et al. [13] produced N–$TiO_2$ using the sol–gel method from the titanium tetraisopropoxide and 1,3-diaminopropane as the titanium and nitrogen precursors, respectively. For the best calcination temperature (500 °C), where the predominant phase was anatase, N–$TiO_2$ revealed greater photocatalytic activity using visible light when compared to Degussa P25. The presence of diaminopropane promoted the formation of a monomeric titanium amine structure which through hydrogen bonding can interact with the neighbor's titanium amines. However, these monomeric structures with little or no cross-linking are weak, and will easily collapse during the calcination, promoting the formation of the rutile phase [13].

## 4. Effect of Nitrogen Incorporation

The incorporation or not of nonmetals such as nitrogen can produce significant changes to the properties of $TiO_2$, which will affect its photocatalytic activity under visible or sunlight radiation [12]. One of the major doubts in this kind of catalyst preparation is related to how N is really incorporated into $TiO_2$ [48–50]. There are some controversial opinions regarding whether nitrogen is really in the $TiO_2$ lattice. In fact, related to nitrogen structure incorporation, some authors have argued that N doping into the $TiO_2$ structure can be interstitial or substitutional [49,50]. This subject can be discussed based on the variations in the diffraction peaks in the XRD pattern, UV-Vis Diffuse Reflectance Spectroscopy (DRS) spectra, Raman spectra, Fourier-Transform infrared spectroscopy (FT-IR), photoluminescence, and X-Ray photoelectron spectroscopy (XPS) analysis compared to pure $TiO_2$. The incorporation of nitrogen will change $TiO_2$ photoactivity mechanisms. Zaleska [48] gave three main explanations for the photoactivity enhancement to visible light with the incorporation of N: the band gap narrowing, the creation of an impurity energy level, or even oxygen vacancies.

The best way to characterize the incorporation of nitrogen into the $TiO_2$ lattice is the compilation of the maximum number of characterization analytical technologies. However, sometimes, it is difficult to gather such a huge amount of data. Therefore, the application of visible light in the photocatalytic degradation of organic compounds can be also helpful to understand if the nitrogen doping was well achieved. In fact, the way that N is incorporated will strongly influence the catalyst band gap [12].

As it can be seen in Figure 1, the band-gap narrowing can occur, which will facilitate the visible light activity due to the introduction of intrabands resulting from the mixing of the 2p states of oxygen from $TiO_2$ with the 2p states of the dopant [51]. Another important feature is the temperature during the preparation of this kind of catalysts [52].

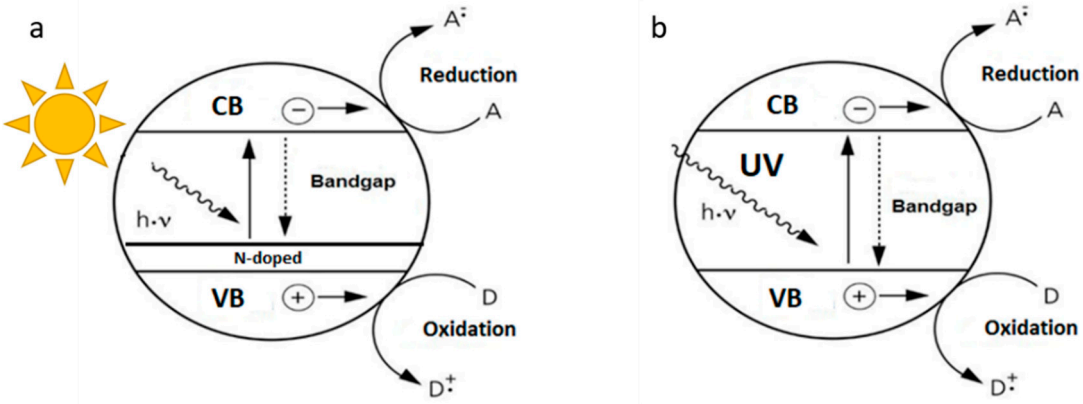


**Figure 1.** Explanation for the band-gap reduction for (**a**) N–$TiO_2$ when compared with undoped (**b**) $TiO_2$.

The nitrogen presence on the $TiO_2$ structure will affect the material phase's crystallinity. For instance, a typical anatase XRD pattern will suffer some deviations. One sign of high crystallinity is the presence of just one phase on the XRD diffractograms. The amorphous phase of $TiO_2$ does not present photocatalytic activity. This can be improved by the calcination of the powder, which promotes the formation of the crystalline phase. This inactivity of the amorphous phase can be related to the recombination between photogenerated electron–hole pairs [53,54].

During nitrogen doping, different temperatures of calcination can be used. Thus, this can affect the crystallinity of the final material [6,13]. Nolan et al. [13] verified that the presence of N enhanced the transformation of anatase into rutile. During pure $TiO_2$ production using a calcination temperature of 600 °C, only anatase remains. The increase of calcination temperature from 600 °C to 700 °C promotes a significant transformation into the rutile phase in both catalysts, but this is higher in the case of N–$TiO_2$. In fact, while the increase for N–$TiO_2$ was from 46% to 94%, for pure $TiO_2$, the transformation was from 0% to 81% [13]. Sun et al. [6] verified that with the temperature increase from 500 °C to 600 °C, rutile formation began (about 7.4%), and from 600 °C to 700 °C, the amount of rutile phase increases until 73.2%, becoming the predominant phase. Moreover, the crystallite size also suffers from modifications due to the calcination temperature. Sun et al. [6] verified a sharpening related to an increase of the crystalline size for the most significant diffraction peak of the anatase phase (1 0 1).

The presence of N onto the $TiO_2$ structure will promote a peak broadening in XRD diffractograms compared to pure $TiO_2$, which indicates a lower crystallite size of nanoparticles [44]. On the other hand, Barkul et al. [15] verified an increase in the crystallite size after nitrogen doping, and concluded that the increasing of the dopant load to at least 7% mol promoted higher crystallite sizes. This increase of the crystalline size was attributed to the higher intensity of the most significant peak (1 0 1). Therefore, no consensus can be found relative to the effect of the presence of nitrogen on the crystallite size. The crystallite size ($D$) is normally determined through the Scherrer equation:

$$D = k\lambda / \beta\cos\theta \quad (1)$$

where $k$ is a shape factor that has a typical value between 0.89–0.94 [6,15], $\lambda$ is the X-ray wavelength, $\beta$ is the full width at half maximum peak (in radians), and $\theta$ is the diffraction angle at which (1 0 1) and (1 1 0) intensity peaks appear [6]. This can be one explanation for these differences in the crystallite sizes, since the $k$ value can be attributed, and this equation just allows an estimate value for this

parameter. Another explanation is the criteria used in these studies to describe the crystallite size: one focused on the peak broadening, and the other on the peak intensity. In order to obtain a complete and more correct approach, the crystallite size must be also analyzed through High-Resolution scanning electron microscope (HR-SEM) or High-Resolution transmission electron microscope (HR-TEM. These two technologies can give more information about the correct crystallite size of nitrogen-doped titanium dioxide particles.

Other changes are related to the shift of diffraction peaks compared to the diffractogram of undoped $TiO_2$. Lee et al. [44] verified that a shift of 0.3° on the higher diffraction peak (1 0 1) can be related to a substitution of oxygen from the $TiO_2$ lattice by a nitrogen atom. This is possible due to the atomic radius of nitrogen, which is higher than oxygen. Ata et al. [55] verified the same shift on this diffraction peak for the sol–gel method of N–$TiO_2$ preparation. The authors noted the typical angle from XRD analysis for anatase as 25.53°, which is a value that decreases with the doping to 25.25°. The same reason as the abovementioned was considered.

The presence of nitrogen with different loads does not change the phases from the pure $TiO_2$ [15]. Barkul et al. [15] concluded that the formation of patterns of nitrogen precursors does not occur. This can be due to the proper substitution of a few sites of oxygen by nitrogen and the low amount of nitrogen usually incorporated [15,56] by the preparation methods.

According to Katoueizadeh et al. [57], the addition of N into the $TiO_2$ structure decreased the crystallization temperature. The authors verified that for the same conditions (100 °C during the sol–gel preparation method), the addition of triethylamine as the N precursor enhanced the formation of the crystalline phase.

Yuan et al. [4] studied different molar ratios of urea/$TiO_2$ (as N dopant)—1:2, 1:1, 3:1, and 5:1—and with different calcination temperatures. The XRD patterns obtained for ratios lower than three was mainly the anatase phase and for ratios 3:1 and 5:1, the phase changes totally to amorphous using the calcination temperature of 350 °C. The authors noted that such a huge amount of urea can block the growth of the crystalline phase during the reaction process. However, the increase of the calcination temperature to 500 °C promoted anatase transformation from the amorphous phase considering the molar ratio of 3:1 and converting it to rutile for temperatures above 600 °C [4]. In the same way, Li et al. [32] verified that the increase in the amount of ethylenediamine as the N precursor promoted the broadening and weakness of XRD peaks, which indicated that N can decrease the crystallinity to enhance the amorphous phase formation. The most significant change was observed in the $TiO_2$ FT-IR spectrum when N is incorporated, which can be due to the presence of bands related to the N–Ti bond vibrations. Normally, these bands can suggest the incorporation of nitrogen into the $TiO_2$ lattice. The typical bands are 1450 $cm^{-1}$, 1365 $cm^{-1}$, 1250 $cm^{-1}$, and 1080 $cm^{-1}$ [44,58,59]. These bands can be found at 1420 $cm^{-1}$, 1270 $cm^{-1}$, and 1170 $cm^{-1}$ [32,60]. Moreover, a sharp tip observed at 455 $cm^{-1}$ can correspond to the O–Ti–O bonding in the anatase phase of $TiO_2$ [61,62]. However, the previous typical bands of pure $TiO_2$ can suffer a shift, which can indicate the presence of N–Ti–N or O–Ti–N [61,63]. Etacheri et al. [61], while preparing N–$TiO_2$ using ethylenediaminetetraacetic acid (EDTA) as the nitrogen precursor, verified a shift from 456 $cm^{-1}$ (undoped $TiO_2$) to 508 $cm^{-1}$. The preparation method was sol–gel and the calcination temperature was 400 °C. The shift was attributed to the incorporation of N into the $TiO_2$ lattice. In the same way, Nolan et al. [13] noted the 508 $cm^{-1}$ peak as a sign of O substitution by N. In this case, the calcination temperatures were 600 °C and 700 °C. Whereas, the authors verified that such a shift did not occur when the calcination temperature was lowered to 500 °C. Thus, Ti–N was not produced at those conditions. This can be due to the different methods or the different nitrogen sources that were used as precursors. On the other hand, sometimes, if the production occurs at room temperature or if the calcination is not well performed, some precursor residues can remain adsorbed on the catalyst surface. These compounds can also be detected in the FT-IR spectrum. For instance, Yang et al. [58], to produce visible-light active N–$TiO_2$ using ethylenediamine as the N precursor, verified the presence on the FT-IR spectra of a vibration band at 1390 $cm^{-1}$, which can be related to $NO_3$ being surface-absorbed. Moreover,

Nolan et al. [13] using the 1,3-diaminopropane as the nitrogen precursor attributed the signals at 1612 $cm^{-1}$ and 1503 $cm^{-1}$ to $NH_2$ vibrations. That data was collected before the catalyst calcination, and the authors noted that this occurs due to the chelating of nitrogen into the titanium metal center.

The calcination temperature appears to be responsible for the removal of organic residues adsorbed on the catalyst surface. However, some authors have noted that high calcination temperatures can promote the elimination of N onto $TiO_2$. Through FT-IR analysis, Li et al. [64] proposed a structure change with the increase of the calcination temperature from 300 °C to 600 °C. At 550 °C, most of the nitrogen was removed, and for 600 °C, the N was totally depleted [64]. According to the XPS analysis mentioned below, at higher calcination temperatures (600 °C), it is still possible to identify interstitial and substitutional N incorporation [4,13]. However, these differences can be related to the type of N precursor that is used.

Other typical bands can appear in this kind of analysis at 1634 $cm^{-1}$ and 3367 $cm^{-1}$. These are related to the bending and stretching vibrations of hydroxyl groups, respectively [13,15]. These vibrations can be associated with the physiosorbed water on the catalyst surface [13,15].

Barkul et al. [15], using two different loads of nitrogen (1% mol and 7% mol), concluded that the high doping amount increased the transmittance (%) due to the higher surface hydroxylation, and noted the presence of hydroxyl groups as an advantage regarding the efficient photodegradation of dye molecules.

XPS analysis allows understanding whether the doped nitrogen was incorporated into the $TiO_2$ structure as substitutional or interstitial [21,50]. The typical binding energy peaks from N 1s are in the range of 396–404 eV for N–$TiO_2$ [50,58,65]. The peaks observed at binding energies between 396–397 eV were attributed to substitutional nitrogen, while peaks between 400–406 eV were related to interstitial nitrogen [13,21,49,50].

Hu et al. [31] verified for the N-doped $TiO_2$ that the N 1s peak was about 399.5 eV. This peak is in accordance with the interstitial nitrogen introduction, since it is near the typical value of 400 eV [50]. In fact, 399.5 eV is significantly above the binding energy corresponding to substitutional N–Ti–N, which is in the range of 396 to 397 eV [49]. Moreover, if nitrogen replaces oxygen, the N 1s binding energy in O–Ti–N is higher than that of N–Ti–N, since the electron density will be reduced [31]. Valentin et al. [50] analyzed the way that N can dope $TiO_2$ and how it reduces the catalyst's band gap. With the interstitial inclusion of N, orbitals associated to the binding energy of 401 eV can appear (O–Ti–N) above the valence band, which will work as support for excited electrons between the valence and conduction bands, allowing visible light absorption [50]. Moreover, Ananpattarachai et al. [21], using three different dopants and the sol–gel method, verified that the incorporation of nitrogen into the $TiO_2$ lattice was interstitial for all of them, with N 1s peaks at the binding energies of 402.5 eV, 406.1 eV, and 402.5 eV for triethylamine, diethanolamine, and urea, respectively. The N 1s peaks attributed to 402.5 eV and 406.1 eV have been considered for nitric oxide (NO) and nitrite ($NO^{2-}$), respectively [50,66].

Nolan et al. [13] verified the effect of the calcination temperature on the N 1s XPS spectra. The increase of temperature from 500 °C to 600 °C did not promote significant changes on the main peak of the XPS spectra for the binding energy of 401 eV, which indicates the interstitial placing of O–Ti–N [13]. On the other hand, Yuan et al. [4] concluded that the increase on the calcination temperature from 350 °C to 600 °C promotes the disappearance of the interstitial peak (401 eV), which means that the high temperatures favored the substitutional introduction of nitrogen. In fact, for the calcination temperature of 350 °C, XPS analysis revealed that the high intensity of the interstitial peak was attributed to absorbed $N_2$ and the small intensity was related to the substitutional peak (396 eV) [4]. Li et al. [64] verified that when ethylenediamine is the N precursor, and 500 °C is used as the calcination temperature, N incorporation is both substitutional (398.3 eV) and interstitial (406.5 eV).

The amount of dopant used in the preparation of the catalyst can also have a relevant impact on the doping processes. The low amount of nitrogen may not be enough to present modifications on

the XPS analysis of N 1s levels. The ratio of urea/$TiO_2$ was analyzed in this ambit, and for the lowest value tested (0.1), no N 1s peaks were observed [4].

XPS analysis can also allow the determination of the real content of nitrogen onto the $TiO_2$ lattice. During the doping processes, different amounts of nitrogen and different ratios between the dopant and the titanium source can be used, but it does not mean that the yield is total, which means that the real amount of dopant should be determined for a better comparison. However, this information is not commonly given.

Yuan et al. [4] verified that for an urea/$TiO_2$ ratio of three, using the calcination temperature of 350 °C over two hours, the doped nitrogen amount was about 20 wt %, and with the increase of the calcination temperature to 500 °C and 600 °C, it is reduced to 2.2 wt % and 0.3 wt %, respectively. Nolan et al. [13] verified the same reduction of N content with the increase of the calcination temperature from 400 °C to 600 °C, which promoted a reduction of nitrogen percentage from 2.09% to 0.14%.

The precursor selected for nitrogen has effects in the real amount that can be incorporated in the N–$TiO_2$. Ananpattarachai et al. [21] concluded that from the initial molar ratio of 1:1 of N:Ti, the percentage of nitrogen content was 4.1%, 0.6%, and 5% when using diethanolamine, triethylamine and urea, respectively. This result is related to the type of amine that is used in the dopant process, since the primary and secondary amines present more N content than the tertiary amine.

A typical undoped $TiO_2$ is active at UV radiation regions below 400 nm. Whereas, typically, catalysts that are well-doped with nitrogen show the maximum absorption for wavelengths above 400 nm. The doped catalyst must show the strongest absorption edge at 400-nm to 530-nm wavelengths to be considered a good photoactive option to be used in the photocatalytic degradation under sunlight radiation [6,67,68]. The energy gap, which is the typical energy of the band gap, is determined by the equation $Eg = 1239.8/\lambda$, where $\lambda$ is the wavelength (nm) of the absorption edge [6,68]. Asahi et al. [26] proposed the N–$TiO_2$ preparation through $TiO_2$ anatase treating under $NH_3$ (67%)/Ar atmosphere at 600 °C for three hours. The authors verified for this catalyst visible light absorption when $\lambda < 500$ nm. Sun et al. [6], using the sol–gel method to dope tetrabutyltitanate with urea, achieved a band gap of 2.58 eV, which represents a significant reduction compared to pure $TiO_2$ (3.02 eV). In the same way, Rizzo et al. [8], using the sol–gel method with titanium tetraisopropoxide and ammonia solution (30 wt %), observed a significant reduction of the band gap from 3.3 eV to 2.5 eV. Moreover, the effect of the addition of different Ti:N ratios can influence the catalyst absorption capacity under visible light and decrease the band gap energy as a consequence. Pérez et al. [69] for the N–$TiO_2$ prepared by the sol–gel method showed that the increase of the theoretical molar ratio of Ti:N from 2:1 to 1:2 enhanced the absorption of light to higher wavelengths. The increase of ratios until 1:2 promoted a decrease on the band gap from 3.19 to 2.51 eV. However, for the molar ratio of 1:1, two different absorption edges appear, where the first corresponds to the undoped fraction, and the second one corresponds to the presence of N onto $TiO_2$ [69]. In fact, Chainorong et al. [70] also identified both UV-Vis absorption edges for N–$TiO_2$ prepared by the hydrothermal method. The first edge was associated with the oxide presence (390–400 nm), and the second one, which was weaker than the first one, was related to the N bonding on the $TiO_2$ lattice [70].

The crystalline phases can have an important role in the visible light absorption due to the wideness of the band gap. Anatase presents a higher band gap compared to rutile. So, rutile is almost able to absorb the visible light [2,3]. As mentioned above, the incorporation of nitrogen into the anatase phase can promote the reduction of the band gap due to the presence of orbitals between the valence and conduction bands [50]. However, the incorporation of N into the rutile crystalline phase promotes the wideness of this band gap [13,50]. The incorporation of N 2p levels reduces the absorption of pure rutile, since it presents a lower energy than the rutile valence band, and the top of the valence band for N-doped rutile was lower than that for pure rutile [50].

Li et al. [64] concluded that the absorption of N–$TiO_2$ was much higher than the pure $TiO_2$ on the visible region due to the presence of nitrogen. This suggests a rearrangement of the energy levels

of $TiO_2$. Hu et al. [31] showed distinct shifts of the absorption bands in the visible light. This can indicate the presence of nitrogen in the $TiO_2$ lattice. In the same way, Nolan et al. [13] verified that for the calcination temperature of 500 °C, it was possible to achieve 100% anatase and a material with high absorption under visible light, which indicates the successful incorporation of N into the $TiO_2$ lattice. However, in this study, the application of high temperatures of calcination (above 600 °C) led to materials with no visible light absorption. This can be related to the band-gap expansion or the nitrogen leaving the $TiO_2$ lattice at those harsh conditions [13]. Besides the calcination temperature, another feature can be relevant to the absorption of visible light or the reduction of the band gap: the calcination time. Rizzo et al. [8] used different times of calcination at 450 °C, and concluded that the time increase from 10 to 30 min led to the band gap decreasing. Contrarily, when the calcination time reached 40 min, the band-gap energy increased again. Therefore, the time of calcination can be an important parameter to enhance the incorporation of nitrogen atoms into the $TiO_2$ lattice and control the band-gap energy of the catalyst.

Yuan et al. [4] revealed that, using an urea/$TiO_2$ ratio of 3:1, an increase in the temperature of calcination promoted the material absorption edge for lower wavelengths. The increase of the calcination temperature may lead to nitrogen desorption or replacement by oxygen onto the $TiO_2$ lattice [4]. The above-mentioned XRD analysis revealed that an increase of the urea/$TiO_2$ ratio decreased the crystallinity of the $TiO_2$, transforming the anatase into an amorphous phase. However, in terms of the absorption edge, the urea/$TiO_2$ ratio increase allowed the use of higher wavelengths [4] to activate the catalyst. The type of introduction of nitrogen onto the $TiO_2$ lattice seems to not affect the band gap. Yuan et al. [4] concluded that the insertion and substitution of nitrogen, which was replaced in the $TiO_2$ lattice, could both contribute to the visible light absorption of the catalyst.

The typical Raman bands of the anatase phase appear at 144 $cm^{-1}$, 197 $cm^{-1}$, 399 $cm^{-1}$, 515 $cm^{-1}$, 519 $cm^{-1}$, and 639 $cm^{-1}$, whereas those related to the rutile phase have been detected at 235 $cm^{-1}$, 447 $cm^{-1}$, and 612 $cm^{-1}$ [8,31,71,72]. Hu et al. [31] verified shifts on the typical bands to 149 $cm^{-1}$, 402 $cm^{-1}$, 521 $cm^{-1}$, 615 $cm^{-1}$, and 642 $cm^{-1}$ for the anatase and rutile phases (50:50 content). However, there are some deviations in the literature regarding the characteristic wave numbers for those crystalline phases in Raman spectra. Rizzo et al. [8] noted that the typical anatase peaks were the ones detected at 141 $cm^{-1}$, 194 $cm^{-1}$, 394 $cm^{-1}$, 515 $cm^{-1}$, and 636 $cm^{-1}$. These values present some deviation from those previously described. Therefore, in order for Raman analysis to be a good technique for analyzing N doping into $TiO_2$, it will be important to compare N–$TiO_2$ Raman spectra with that obtained for pure $TiO_2$ produced by the same method. The quantum size effect of nanoparticles of N–$TiO_2$ can promote slight shifts on the Raman band [73]. This is the most typical response found in the literature that mentioned the incorporation of N into a $TiO_2$ lattice. Pérez et al. [69] analyzed the Raman spectra for the different molar ratios of Ti:N for N–$TiO_2$ produced by the hydrothermal method. These authors concluded that for 2:1 and 1:1, the shift of the peaks to lower values correspond to the incorporation of N into the $TiO_2$ lattice [69]. On the other hand, Rizzo et al. [8] verified a shift from the typical signal of anatase from 141 $cm^{-1}$ to 144 $cm^{-1}$ when characterizing N–$TiO_2$, and related this to the change of the oxygen stoichiometry due to the presence of nitrogen. Some controversy can be found regarding this characterization. In fact, the shift of typical peaks to the lower or higher values may be a sign of N incorporation in the $TiO_2$ lattice [8,31,69,74,75].

N incorporation in $TiO_2$ can reduce the electron–hole recombination effect, which improves its photoactivity. In fact, Lee et al. [44] verified that the undoped $TiO_2$ presents a higher intensity of photoluminescence compared to N–$TiO_2$. The Raman peaks can also help identify the crystal size of doped $TiO_2$, working as complement of the XRD analysis. Kassahun et al. [75] verified a decrease in the intensity of the 144 $cm^{-1}$ peaks of N–$TiO_2$ compared to pure $TiO_2$, which means a lower crystal size in accordance to the XRD analysis.

Since in the literature, the way that N is incorporated into $TiO_2$ is controversial, there is the need to combine the characterization data (as discussed in this section) from several analytical techniques to assure the success of the catalyst preparation method. Besides, in the wastewater treatment field,

the best way to select a catalyst preparation process should rely on the screening of several materials by testing their efficiency and stability on the photocatalytic degradation of organic contaminants under visible/sunlight irradiation. These data should complement the characterization of the materials.

In this context, Table 2 shows some typical modifications that can occur with the incorporation of nitrogen in the $TiO_2$ structure through several analytical methodologies that are used for the characterization of catalysts.

**Table 2.** Main changes identified through different characterization techniques due to N incorporation in $TiO_2$.

| Analytical Technique | Main Characteristics | Reference |
|---|---|---|
| **XRD** | -N enhances anatase transformation into rutile<br>-N promoted 0.3° shift on (1 0 1) diffraction peak<br>-No N diffraction peak is detected<br>-N precursor and N:$TiO_2$ ratio have complex relation with crystallinity | [13]<br>[55]<br>[15,56]<br>[4,25,32,43] |
| **FT-IR** | -$TiO_2$ typical bands: 1450 $cm^{-1}$, 1365 $cm^{-1}$, 1250 $cm^{-1}$, 1080 $cm^{-1}$<br>-N–$TiO_2$ typical bands: 1420 $cm^{-1}$, 1270 $cm^{-1}$, 1170 $cm^{-1}$ (suggest N in $TiO_2$ lattice)<br>-455 $cm^{-1}$: O–Ti–O (anatase) can be shifted due to N–Ti–N and O–Ti–N<br>-$TiO_2$: 456 $cm^{-1}$ shifts to 508 $cm^{-1}$ (N–$TiO_2$) | [32,43,58–60]<br>[61–63]<br>[61] |
| **XPS** | -Binding energy: 396–397 eV (substitutional N) and 400–406 eV (interstitial N) | [13,21,48,50,58,65] |
| **UV-Vis DRS** | -$TiO_2$ absorption $\lambda \leq 400$ nm<br>-N–$TiO_2$ absorption $400 \leq \lambda \leq 500$ nm<br>-N:$TiO_2$ ratio affects band gap<br>-Calcination temperature and time affects band gap | [6,67]<br>[69]<br>[8,31,52,76,77] |
| **Raman** | Shift of the typical $TiO_2$ bands to lower values related to N incorporation into lattice | [8,31,69,74] |
| **Photoluminescence** | N–$TiO_2$ shows lower photoluminescence than $TiO_2$ | [44] |

## 5. Effect of N–$TiO_2$ Co-Doping

N–$TiO_2$ shows, as described above, some advantages regarding band-gap reduction, which would allow the utilization of visible light and/or sunlight radiation in photocatalytic degradation processes. The presence of other dopants can place a mid-gap between the valence and conduction band, which permits the reduction of the typical band gap of $TiO_2$ [78,79]. On the other hand, some dopants are not able to reduce the band-gap width [45]. For example, fluorine does not change the $TiO_2$ band gap, since the p orbitals of F present lower energy than those from oxygen atoms [45]. However, F shows higher electronegativity when compared to O, which will allow a better trapping of electrons, promoting the separation of electron–holes pairs and minimizing the recombination phenomena. This may enhance photocatalytic degradation [45,80]. Moreover, the synergetic effect of different ions from two or more nonmetals can enhance the separation of photogenerated holes and electrons, reducing the recombination phenomena [19,59]. In fact, some works have even reported some cases of tri-doped materials [19,62]. In this case, the efficiency improvement at visible light should be related with the increase of the surface acidity, band-gap narrowing, and the reduction of electron–hole recombination [62,81,82].

The effect of the co-doping process can be analyzed in terms of the degradation of contaminants, since sometimes, no significant differences are found in the characterization of the catalyst compared to N–$TiO_2$. Thus, normally, in order to understand the real effect of co-doping, N–$TiO_2$ should be compared with the co-doped catalysts regarding their performance related to the removal of pollutants.

N–$TiO_2$, S–$TiO_2$, and N, S–$TiO_2$ were successfully prepared using the sol–gel method at room temperature for the degradation of methylene blue and phenol [59]. Syafiuddin et al. [59] verified that

N, S–$TiO_2$ was the best catalyst using the visible light for methylene blue and phenol degradation after six hours. Besides the higher photoactivity, another reason for the best performance can be related with the high specific surface area of this catalyst [59].

N, S co-doped $TiO_2$ can be very often found, since during the catalyst preparation method, thiourea (a source of both S and N) is generally used as a precursor. This can also present advantages in terms of band-gap reduction [12,76], allowing the best photocatalytic performance when using visible light. Brindha and Sivakumar [79] found that the N, S co-doped $TiO_2$ prepared by the hydrothermal method verified no significant changes on the XRD patterns when compared to the anatase phase of $TiO_2$. In the same way, Li et al. [32] verified that the incorporation of N and S onto the $TiO_2$ structure using thiourea as an N and S source does not promote modifications on the crystalline phase of pure $TiO_2$.

Sun et al. [6] co-doped N–$TiO_2$ with different amounts of Ce (0.3% mol, 0.6% mol, and 1.2% mol) using cerium nitrate as the precursor. The initial change in the N–$TiO_2$ is the disappearance of the rutile phase with the presence of Ce. In fact, Ce has an inhibitory activity for the transition from the anatase phase to the rutile phase [6]. The radii of $Ce^{4+}$ or $Ce^{3+}$ (0.093 nm and 0.103 nm, respectively) are larger than that for $Ti^{4+}$ (0.064 nm), which will promote lattice distortion and expansion when Ce is in the $TiO_2$ lattice. Moreover, a reduction of the crystallite size is also verified for increasing Ce amounts [6]. In fact, the increase of the cerium amount on N–$TiO_2$ reduces the crystalline size, since the most significant peak of anatase suffers from broadening [6]. The same response was verified with the presence of nitrogen compared to pure $TiO_2$ [44]. Shen et al. [83] verified the inhibition of the anatase transition to the rutile phase during the calcination of N, Fe–$TiO_2$ produced via the sol–gel method. Although N–$TiO_2$ calcinated at a temperature of 600 °C reveals a fraction transition of the anatase phase to the rutile phase, only the anatase phase is detected for N, Fe–$TiO_2$, even when calcinated at higher temperature. Thus, the presence of the co-dopant inhibits phase transition. Nkambule et al. [84] prepared N, Pd–$TiO_2$ by the sol–gel method using ammonium hydroxide and palladium diamine dichloride as precursors of N and Pd, respectively. The presence of a PdO peak at the 2θ value of 33.8° was verified through XRD. Moreover, sharp and intense anatase peaks revealed crystallinity improvement. On the other hand, the typical anatase peaks from Raman analysis do not suffer changes, which can be related to the low amount of dopant used [84].

FT-IR analysis is important to verify whether the co-doping occurs at the lattice, establishing bonds with Ti or O. The presence of S on the N–$TiO_2$ lattice can be identified by the peak detected at 1055 $cm^{-1}$, which can be attributed to the Ti–O–S bond [79,85]. On the other hand, the peak at 1217 $cm^{-1}$ can be attributed to the surface-adsorbed $SO_4^{2-}$, which is the result of some unreacted precursor [59].

XPS analysis enables drawing conclusions about the chemical states of the different species considered in the N co-doped $TiO_2$. Sun et al. [6] analyzed the peaks of $Ce^{4+}$ and $Ce^{3+}$ for different states of Ce such as $Ce3d_{5/2}$ and $Ce3d_{3/2}$. For $Ce^{3+}$, the typical binding energy peaks for $Ce3d_{5/2}$ and $Ce3d_{3/2}$ can be detected at 885.3 eV and 904.1 eV [86]. Whereas for $Ce^{4+}$, the binding energy peaks for $Ce3d_{5/2}$ and $Ce3d_{3/2}$ can be found at 881.9 eV and 898.2 eV [86]. After the photocatalytic reaction, the peak area of $Ce^{3+}$ was reduced significantly, which means that the majority of these ions were oxidized to $Ce^{4+}$ and worked as hole traps, minimizing the recombination, and therefore allowing the enhancement of the photocatalytic activity for the degradation of contaminants [6]. Nevertheless, this conversion does not mean a reduction of the amount of Ce ions; on the contrary, in this study, the Ce amount remains almost the same, which means that this co-doped catalyst presented a good stability [6] in what is regarded as the Ce-leaching effect. Sun et al. [6] also analyzed the binding energies of N 1s states for this co-doped catalyst. The peaks were found for 369.9 eV, 399 eV, 400.3 eV, and 402.4 eV. The signal of 396.9 eV is normally related to the substitution of O by N atoms, ascribing to Ti–N bonds [6,26]. These results are in accordance with the FT-IR analysis for the Ce, N–$TiO_2$, as described above [6]. Moreover, the peak at the binding energy of 399 eV corresponds to the O–Ti–N. Thus, this is related to the interstitial introduction of N onto the $TiO_2$ lattice [6,87]. This peak (399 eV)

also presents the highest intensity of N 1s due to the lowest electron density around N, since the presence of oxygen, which has a higher electronegativity, will attract the electrons more intensively [6]. On the other hand, the remaining peaks (400.3 eV and 402.4 eV) can be related to the accidental presence of N atoms onto the surface of the samples, which could represent the N–N, N–O, or NHx bonds [6,88].

Guo et al. [45] produced N, F–$TiO_2$ by three different sol–gel methods with changes to the operating conditions, and analyzed the XPS spectra for the N 1s and F 1s states. For all the methods, the N 1s has its main peak at the binding energy of 396 eV, which suggests that N incorporation occurs via the substitutional way with the formation of O–Ti–N bonds. In the case of F 1s, the binding energy is located between 681.1–680.4 eV, which indicates a substitutional placement of F onto the $TiO_2$ lattice [45]. Moreover, the three different methods do not promote significant changes on the binding energy peaks, but rather can influence the amount of N and F that is doped. Guo et al. [45] verified an increase in the N and F doping doses when using the first method compared with the two other methods, as described above. N, Fe–$TiO_2$ presents peaks for N 1s states at binding energies of 399.7 eV and 396.7 eV, which means that the incorporation of N onto the $TiO_2$ lattice occurs via interstitial and substitutional mechanisms [83]. On the other hand, Fe was not incorporated into the $TiO_2$ lattice, since the peak of Fe 2p was about 710.6 eV, and corresponded to Fe $2p_{3/2}$ for $Fe_2O_3$, which means that the ferric nitrate was converted into iron (III) oxide during the calcination [83]. Nkambule et al. [84] used XPS to analyze the incorporation of Pd and N onto the $TiO_2$ lattice. According to the authors, the N 1s state was not observed due to the low amount of N used, which might have been below the detection limit. Alternatively, it is even possible that Pd can be at the N defect sites, blocking the detection. The peaks of Pd $3d_{5/2}$ (335.6 eV) and $3d_{3/2}$ (341.6 eV) reveal that Pd can be in metallic Pd and/or PdO form (in accordance with the XRD analysis). Besides, the Pd 3s signal (671.2 eV) indicates a small amount of Pd in the catalyst. Therefore, the authors cannot assure whether the Pd is interstitially or substitutionally placed onto the catalyst lattice.

UV-Vis DRS should be analyzed in order to understand the modifications imposed by the co-doping in the light absorption capacity. Using this method, Li et al. [32] compared the absorption of N–$TiO_2$ and N, S–$TiO_2$, revealing that the absorption at the visible region was higher for the N–$TiO_2$ catalyst. The presence of S reduced the absorption edge, which means a lower reduction of the band gap in the N, S–$TiO_2$. One of the explanations for this can be that S belongs to the same group as O. This substitution of O by S on the $TiO_2$ lattice may be preferred when compared to N replacement. Thus, S will compete with N for O replacement on the $TiO_2$ lattice. Moreover, N presents a more similar atomic radius with O (65 pm and 60 pm, respectively), unlike S (100 pm), which will inhibit the substitution of nitrogen on the $TiO_2$ lattice.

Sun et al. [6] used Ce as the co-dopant of N–$TiO_2$, and verified a significant reduction of the band gap compared to pure $TiO_2$. In fact, the band-gap energy decayed from 3.02 eV (pure $TiO_2$) to 2.52 eV (Ce, N–$TiO_2$). Still, the difference is not so high compared with the band-gap energy of N–$TiO_2$, in which the value was 2.58 eV. The substitution of O by N to promote the formation of Ti–N (nitride) and the synergistic effect between the 4f orbital of Ce were identified as the main factors responsible for the visible region absorption enhancement in this catalyst [6]. Shen et al. [83] verified that the presence of Fe as the co-dopant does not interfere on the N–$TiO_2$ absorption spectra. In fact, the band gap of the co-doped materials was 2.22 eV, while for the N-doped materials, it was 2.24 eV. Nkambule et al. [84] observed that the presence of N and Pd onto $TiO_2$ promotes the decrease of the band gap from 3.15 eV to 2.48 eV. However, the authors did not analyze the impact of N and Pd separately, which means that the band-gap reduction can be related to the presence of N onto the $TiO_2$ lattice.

As it happens for N–$TiO_2$, the use of a co-dopant may lead to changes in terms of the material Raman spectrum. The typical changes are the shifting of the common Raman peaks of $TiO_2$. Brindha and Sivakumar [79] verified Raman peaks shifts from 519 to 513 $cm^{-1}$, 399 to 396 $cm^{-1}$, and 197 to 194 $cm^{-1}$ for N, S co-doped $TiO_2$ prepared by the hydrothermal method. The authors related this change to N, S-doping, but did not discuss the roles of N and S on this perturbation. As noted before,

N also promotes a shift on $TiO_2$ Raman peaks, but for higher instead of lower values [31]. Thus, the shift for lower values can be due to the presence of S on N–$TiO_2$.

The co-doping with noble metals (Pd, Pt, Au, and Ag) can enhance the photocatalytic activity, since these metals have the capacity to absorb the visible light due to the surface plasmon resonance [16]. Moreover, Pt onto the $TiO_2$ lattice acts as an electron sink from the $TiO_2$ conduction band, facilitating electron transfer to adsorbed oxygen [89]. Nkambule et al. [84] verified that Pd co-doped onto N–$TiO_2$ enhances the photocatalytic oxidation of natural organic matter from water. Jurek et al. [90] prepared N–$TiO_2$ co-doped with Pt using a sol–gel method with different atomic ratios of Ti:N (1:1, 1:2, 1:4, 1:10). For this, N–$TiO_2$ was firstly prepared from urea and titanium tetraisopropoxide using different Ti:N ratios. Then, $K_2PtCl_4$ was added and stirred with the N–$TiO_2$ suspension for 12 h, followed by further calcination at 400 °C for one hour. The increase of the Ti:N ratio to 1:4 promoted the decrease of the band gap from 3.1 eV to 3.05 eV. Nevertheless, for higher ratios, no significant modifications were detected. On the other hand, the addition of Pt promoted a decrease of the band gap to 2.95 eV for a Ti:N ratio of 1:1. The further increase in the Ti:N ratio increased the band gap [86]. The incorporation of N onto $TiO_2$ was interstitial, due to the chemisorbed species such as $N_2$ or NO. This was determined by XPS analysis. However, many studies can be found in the literature where authors have noted that higher photocatalytic activity can be achieved in the absence of substitutional N incorporation, but just only with the interstitial placement [39,91]. The higher photoactivity of Pt–N–$TiO_2$ was related to the easier electron transfer from the conduction band to oxygen, which enhanced the superoxide generation [90].

Shen et al. [83] concluded through data from multiple analytical techniques that in the preparation of N, Fe–$TiO_2$, N was incorporated in the $TiO_2$, while Fe was adsorbed on the catalyst surface. Despite this, the authors verified the positive effect of co-doping into methyl orange conversion, and concluded that the presence of Fe on the $TiO_2$ surface enhanced its photocatalytic activity, since it reduces the electron–hole recombination phenomenon and increases the photo quantum efficiency. Teh et al. [92] produced co-doped N, Cl–$TiO_2$ via a sonochemical sol–gel method. The authors verified the effect of the N, Cl:Ti ratio (from 0.5 to 4), and concluded that the increase on the N, Cl load until two promotes the decolorization of Reactive Black Five. According to the authors, this improvement is specifically related to the increase on the Cl amount onto the $TiO_2$ lattice, since chlorine enhances the surface acidity [92]. Moreover, for N, Cl:Ti ratios from 2:1 to 4:1, a decrease of the decolorization rate was observed. The pointed reason was related to the high load of N, which can decrease the number of active sites onto the catalyst surface [92]. Nevertheless, these authors never analyzed the doping effect of N and Cl onto $TiO_2$ separately to understand the real impact of each dopant on the decolorization, as well as the catalyst characterization.

## 6. Relevant Parameters of N–Doped $TiO_2$ Photoactivity

Several studies have indicated that the most representative characteristics for the definition of a good N–$TiO_2$ semiconductor catalyst is the reduced particle size, a good dispersion of nitrogen onto the structural geometry of a $TiO_2$ lattice, a high surface area, the quantum size effect, crystalline phases, and the hydrophilicity of the catalyst surface [31,44]. These parameters are typically evaluated using XRD analysis.

As mentioned above, the doped nitrogen can be regarded as interstitial or substitutional according to the N position on the crystalline structure. Peng et al. [30] verified that the interstitial N–$TiO_2$ is more visible light-active than the substitutional N–$TiO_2$.

A quantum size effect for particles smaller than 10 nm promotes the band-gap extension, which would allow a better exploitation of the potential of photogenerated electron–hole pairs [31,93]. The increasing of active sites on the surface can occur through the reduction of the particle size or an increase of the specific surface area [31,94]. The crystallinity can be improved with the calcination temperature and with other preparation steps such as the use of ultrasound irradiation [43,95–97].

A hydrothermal method, using urea as the nitrogen precursor and titanium tetrachloride as the titanium dioxide source, can produce a well-dispersed N–$TiO_2$ with ultrafine particle sizes (about five nm) [31]. This catalyst has also the same amount of anatase and rutile phases as a particularity, since anatase is normally the predominant phase [32]. This ultrafine catalyst revealed greater performance than the commercial P25 on the decolorization of a reactive Brilliant Blue KN–R aqueous solution under visible light and UV light using a 110-W high-pressure sodium lamp and a 125-W high-pressure mercury lamp, respectively. According to the results, this high performance is related with N doping and the usage of PEG-4000, which improves the dispersion of $TiO_2$ particles [31].

Another important feature that can also be related with the good results of N-doped $TiO_2$ is the hydrophilicity of its surface [5,44,98]. The surface hydrophilicity makes the photocatalytic activity under visible light irradiation possible [20,44,58,99]. In order to improve the hydrophilicity of the catalyst surface, some different methods can be used, such as UV radiation, visible light radiation, plasma treatments, and acid treatments [5,44,98]. As an example, visible light radiation was analyzed to test the potential of this parameter on the photocatalytic activity enhancement. A sol–gel method process aided by ultrasound irradiation was used to prepare a nanoporous N–$TiO_2$ catalyst (with titanium butoxide and urea as the $TiO_2$ and N precursors, respectively). After preparation and drying, the N–$TiO_2$ was irradiated for one hour using a solar simulator equipped with a 150-W Xe lamp [44]. Regarding catalyst characterization, no significant changes were verified regarding the XRD pattern and crystallite size when comparing N–$TiO_2$ with and without visible light radiation. However, a significant change was verified on the surface energies obtained through the contact angle data of test liquids (deionized water, ethylene glycol, and n-hexane) using the extended Fowkes' equation to transform the data. The calculations reveal that the surface free energy of N–$TiO_2$ radiated with visible light was 154.71 $mJ/m^2$, while for unirradiated N–$TiO_2$, this value was significantly lower (91.47 $mJ/m^2$). This difference is related to the formation of surface hydroxyl groups during this process [44]. Another aspect is the low intensity of photoluminescence analysis, since the high amount of hydroxyl groups at the surface will accept more holes to form hydroxyl radicals and minimize the recombination of electron–hole pairs [44]. Therefore, the high photocatalytic activity of this hydrophilic catalyst is correlated with the larger amount of hydroxyl groups at the catalyst surface.

Powder catalysts are still widely used in photocatalytic processes to reduce mass transference limitations, which is how they also increase the reactors' performance. However, powder dispersion inside the reactors should be as perfect as possible to take advantage of the reactor volume so that the photocatalytic process performance for the contaminant's degradation may be maximized. Moreover, these small particles, which typically have large surface areas, can agglomerate due to the attraction of Van der Waals forces coupled with electrostatic and steric stabilization, since the adsorbed organic substance at the nanoparticle surface can attract other nanoparticles [100,101]. In fact, other factors, such as ions, pH, and the amount of catalyst, may lead to modifications at the material surface and change the stability of the nanoparticles. The aggregated size that can occur at these specific conditions can promote a reduction in the photocatalytic efficiency. Indeed, besides leading to the reduction of the active surface area, it can also promote light scattering and consequently reduce light propagation [100]. Some authors have noted the aggregate size as the factor that is most responsible for the reduction of the degradation ability of a catalyst [8,38,100]. Vaiano et al. [100] analyzed the trimodal aggregate distribution, with aggregate sizes ranging between 0–3000 μm, and compared the effect with that of the presence of an organic species working as a dispersing agent. This dispersant changed the size distribution to monomodal, ranging from 0.1 to 2 μm. The authors verified that at the presence of the dispersant agent (10 ppm), N–$TiO_2$ (3 g/L after 120 min using visible light irradiation), it was possible to reach a better methylene blue degradation (80%) when compared to the results obtained when no dispersant was applied (50%) [100]. The amount of catalyst can have a relevant impact on the aggregate size. Vaiano et al. [100] verified that the increase of the catalyst amount from 3 to 6 g/L, using the same amount of dispersant agent (10 ppm), promoted a decrease on the methylene blue decolorization. In fact, the aggregate size increased with the increasing catalyst concentration. Moreover, after four

cycles of 15 min of catalyst reuse at the presence of the dispersant agent, no efficiency reduction was observed on the methylene blue decolorization using visible light irradiation [100]. Therefore, another feature that was taken in consideration in these processes is the amount of catalyst for the degradation of photocatalytic contaminants. The optimal concentration must consider the beneficial ratio between amount and efficiency. This is also substantially important regarding light scattering. Another way of minimizing the aggregation of nanoparticles can be the use of carbon nanotubes and graphene over the $TiO_2$ structure due to the strong and intimate interaction between titania and carbon materials [20,102].

The use of ultrasounds during the preparation of catalysts through the sol–gel method can influence the formation, growth, and crystallization of the anatase phase through the increase or decrease of cavitation activity [92,103,104]. The power and time of ultrasonication were analyzed by Nepollian et al. [103]. These authors verified that the increase of the ultrasonication time from 30 to 90 min decreased the anatase phase, and thus increased the rutile and brookite phases. Alongside these effects, the crystalline size decreases as well, which promotes an increase of the catalyst-specific surface area. However, 120 min of sonication seems to have the opposite effect. The increase of the power density from 18 to 42 W/L endorses a decrease of the anatase fraction to form rutile and brookite, while also increasing the crystalline size and decreasing the specific surface area. Moreover, the changes promoted on these parameters are intimately related with the degradation efficiency of 4-chlorophenol. The increase of the ultrasonication time (up to 90 min) and the power density both enhance the degradation of 4-chlorophenol [103].

Teh et al. [92] used co-doped N, Cl–$TiO_2$ to verify the effect of a wide range of preparation parameters such as the presence or absence of ultrasonication on the decolorization of Reactive Black Five. The preparation time and power density increase the decolorization capacity up to a certain point. The presence of ultrasonication during the sol–gel method seems to enhance the catalyst capacity of visible light absorption when compared with the sol–gel preparation involving stirring. This can be related to the higher capacity of ultrasonication to recover more N and Cl onto the $TiO_2$ lattice due to the production of hotspots from the collapse of cavitational bubbles during sonication [92]. Moreover, the surface acidity of the catalyst can be a relevant parameter for this type of material, depending on the type of organic molecule tested [105,106]. High surface acidity can increase the photocatalytic activity for the polar molecules, since it enhances their adsorption on the catalyst surface, which will favor their oxidation [92,106].

Teh et al. [92] verified that the catalyst calcination temperature had a large impact on the decolorization of Reactive Black Five when ultrasonication was used as the catalytic material in the co-preparation method. Increasing the calcination temperature from 200 °C to 600 °C promotes a significant decrease of the decolorization efficiency. This could mean that the Cl in interstitial positions on the $TiO_2$ lattice disappear when the temperature increases. Moreover, for stirred prepared samples, the decolorization efficiency increases when the calcination temperature increases from 200 °C to 400 °C [92], which means that the incorporation of N and Cl onto the $TiO_2$ lattice occurs. This confirms that the stirring method without calcination was not able to introduce the Cl onto the $TiO_2$ lattice; meanwhile, for ultrasonication, the placement of Cl would be interstitial, and therefore was removed as the temperature increased.

## 7. More than Powder

One of the main questions when investigating potential industrial applications for this kind of catalyst is related to its recovery and reuse. When using powder materials, this will imply expensive particle-separation processes after treatment. Therefore, considering the recovery of the catalyst, in the literature, studies can be found that are related to the immobilization of doped $TiO_2$ on suitable supports or even $TiO_2$ nanostructures, such as nanotubes arrays supported on titanium foils [106–109]. The immobilization of doped $TiO_2$ can occur in different types of substrates such as hollow glass spheres [110], reactor walls [111], membrane reactors [112], synthetic polymers [55,113,114], and graphene [79]. The most used methods for supporting titanium dioxide

particles on a suitable substrate is dip coating (or the sol–gel method) [115], chemical vapor deposition [116], the hydrothermal method [117], and the solvent-casting method [55]. This kind of catalyst can present advantages for continuous processes, which will allow the industrial application of photocatalytic processes, and reduce the implementation of separation processes and thus operating costs. However, in terms of efficiency, decay may occur when compared to the powder forms of $TiO_2$. In fact, the number of active sites will be reduced compared to powder, since the support will cover only one side of the $TiO_2$ surface.

The above analysis characterized the dopant presence, and can help understand whether the application of the support was successful or not. This means analyzing whether or not the photocatalytic characteristics were lost during the preparation of the support. As noted, the support will generally lead to an efficiency decrease compared to unsupported N–$TiO_2$. One way to keep the supported catalyst very active is using higher amounts of powder to totally cover the support. Ata el al. [55] applied a solvent-cast method to support N–$TiO_2$ on a polystyrene surface after using a sol–gel method to prepare the doped titanium dioxide, which involved applying ammonia as the N precursor. In this study, significant changes on the Raman and UV-Vis DRS spectra were verified upon the presence of a polystyrene support, when considering a low of amount of N–$TiO_2$ near the support. For example, the polystyrene has Raman typical bands at 998 $cm^{-1}$, 1026 $cm^{-1}$, and 1599 $cm^{-1}$, which suffer a decrease in their intensity upon using 0.015 g of N–$TiO_2$. However, this decrease disappears when using higher loads of catalyst (0.05 g, 0.1 g, 0.2 g, and 0.3 g) on the support [55]. This indicates that the support surface was totally covered by the N–$TiO_2$ particles for those powder loads. Horovitz et al. [112], using a membrane coating, also verified differences with the amount of N–$TiO_2$ that is coated. The authors used a porous commercial $Al_2O_3$ membrane and coated 78% to 84% of its surface with N–$TiO_2$, which enabled the use of sunlight radiation for the photocatalytic degradation of carbamazepine. Surface characterization revealed that the incorporation of N into the coated structure was mainly interstitial, and the maximum atomic N content that was obtained was 0.9%. This coating was performed using a pipette drop-coating method, which promoted an about 50% reduction in the membrane permeability for the 200-nm pore size. However, this placement of N–$TiO_2$ inside the pores can present advantages regarding the contact of the contaminants, in which the active sites increase the photocatalytic degradation [112]. To improve the mass transfer onto the catalyst surface inside the membrane pores, the authors proposed a water flux and/or residence time increase [112]. However, an increase in water flux can be a problem due to the limitations of the membrane, and the residence time can be a problem when treating high-flow rates, since big reservoirs would be required to avoid the threat of excess volume.

The need to increase the amount of powder to upload onto the support is a drawback of these kinds of processes, since the support is usually a very porous material, and will need a great amount of powder so that the supported catalyst can be active for contaminants degradation under visible light. In this way, the amount of N–$TiO_2$ that is used can be higher compared to the amount needed for the degradation of contaminants when it is used in powder form. However, Ata et al. [55] verified for the same amount (0.2 g) of N–$TiO_2$ that the presence of the support did not influence the decolorization of methylene blue (MB) when compared to powder N–$TiO_2$. This means that the support did not introduce diffusional limitations to the process, which is an advantage. The reuse capacity of this supported catalyst should also be analyzed as an important feature, since the main advantage of this kind of catalyst is avoiding the processes that separate particles from liquid after treatment. The number of cycles should be carefully selected to prove the stability of the supported catalyst. Besides, the possibility of N–$TiO_2$ leaching from the support must be considered, as well as the leaching of nitrogen from titanium dioxide nanoparticles, if the doping was not well established. Ata et al. [55] verified a slow decrease in the efficiency of the decolorization process after four cycles of reuse, and noted that this decrease was a consequence of the weakening of the dye absorption ability. Therefore, the reuse stability should be analyzed for a higher number of cycles. Moreover, the changes to the characteristics of the catalyst after use must also be assessed. For instance, besides

understanding the effect of some contaminants or the degradation of dyes, it will be important to characterize the used catalyst regarding UV-Vis DRS, since changes in the catalyst absorption spectrum can occur after use. Another way to detect the activity of this kind of catalyst is to study their effect on the degradation of contaminants. This way, it is possible to understand whether the support inhibits the photocatalytic degradation of doped $TiO_2$ more than the powder. Ata et al. [55] verified the effect of different amounts of N–$TiO_2$ (0.015 g, 0.05 g, 0.1 g, 0.2 g, and 0.3 g) on the support regarding the photocatalytic decolorization of methylene blue (MB) under visible light with three eight-W lamps over three hours, and compared it with an empty support. The profiles of degradation were enhanced as the mass of the N–$TiO_2$ that was used increased. The empty support did not promote a significant decolorization of MB. Otherwise, the supported catalysts prepared with 0.015 g of N–$TiO_2$ presented the worst result (about 50% decolorization), which can be related to the low amount of N–$TiO_2$ at the surface of the support. This is in accordance with the characterization of catalysts through Raman and UV-Vis DRS analysis [55], since, as shown before, the characteristic peaks of the support were still detected for this load. Brindha and Sivakumar [79] detected a significant reduction of the efficiency of the decolorization of dyes as the amount of graphene that was used as a support of N, S–$TiO_2$ increased (7.5% and 10%). This was related to the masking of the active surface of $TiO_2$, which inhibits the active sites. This is also in accordance with the results of UV-Vis DRS, in which it was possible to observe an increase of the supported catalyst band gap when a higher amount of graphene was applied [79].

Moreover, the supporting procedure is an additional step that involves costs. The supporting method, as well as the support material, should be selected in accordance with the application. For instance, most of the polymers that can be used for supporting N–$TiO_2$ did not work with photocatalytic ozonation. Ozone can destroy the polymer, leading to the decomposition of the catalyst and the contamination of water. Therefore, the catalyst application technology should be taken into consideration when the support is selected.

Alternative methods can be found to address the problems regarding the preparation and stability of the polymeric-supported N–$TiO_2$. $TiO_2$ nanotubes resulting from the anodization of Ti foils is one example. In this preparation method, Ti foils work as anode, and platinum mesh works as cathode [108,109]. Then, these foils can be used in continuous processes, thus avoiding a posterior separation technique. However, a major drawback of $TiO_2$ nanotubes is their large band gap, which typically requires UVA radiation, and does not enable suitable activity under visible light or even using sunlight radiation. One possibility is doping it with nitrogen in one or two steps. The synthesis by two steps consists firstly of the production of structures of $TiO_2$ nanotubes, and then, as a second step, the incorporation of nitrogen by annealing the nanotubes with ammonia at high temperatures [116,117]. Also, the hydrothermal treatment of $TiO_2$ nanotubes may be a way of incorporating N [118]. Alternatively, with one-step synthesis, nitrogen is incorporated during the anodization method, which is used in the production of nanotubes [7,108,109,119]. In this case, the production of nitrogen-doped $TiO_2$ nanotubes is based on the presence of urea, ammonium nitrate, and hydroxide; alternatively, they are produced by the anodization of TiN alloy [7,119] coupled with the electrolyte. However, the most common nitrogen precursor is urea, due to the low cost of its effective preparation method [108]. Antony et al. [7] produced N–$TiO_2$ nanotubes using different amounts of urea coupled with an electrolyte containing $NH_4F$, water, and ethylene glycol. The authors observed a slight shift in the positions of XRD peaks for values higher than 2θ, indicating the lattice deformation of $TiO_2$ due to nitrogen doping. Moreover, the XPS analysis for the N–1s state indicated the existence of different N environments. This means that nitrogen was incorporated into the lattice by both interstitial and substitutional methods. However, the authors noted that the substitutional method is predominant [7]. In this study, the catalyst activity under visible light was not tested, but the effect of different nitrogen loads on the optical band gap were analyzed, which decreased while increasing the N concentration [7]. Maziesrki et al. [108] produced N–$TiO_2$ in a similar way, and verified some changes on the electronic properties of the material. Besides, the authors also studied the

effect of this kind of catalyst on phenol degradation under visible light irradiation. In terms of catalyst characterization, the increase of N concentration (0.1%, 0.3%, and 0.5%) onto N–$TiO_2$ nanotubes promoted the decrease of the band gap from 3.0 to 2.75 eV.

Other authors have supported $TiO_2$ with graphene and carbon nanotubes [20,79,102]. These supports can also present advantages regarding charge separation in the semiconductor catalysts [20,102]. For example, graphene sheets can work as electron acceptors, thus reducing electron–hole recombination [120]. Moreover, the reduced graphene oxide can offer the possibility of using the hydrothermal method to incorporate N and S onto its lattice using thiourea as the precursor. This increases its photocatalytic efficiency using visible light [79]. In terms of catalyst characterization, this kind of material can present significant differences compared to the typical behavior for $TiO_2$. For example, Brindha and Sivakumar [79] verified the presence of graphene on the Raman and FT-IR spectra through SEM analysis. Therefore, the characterization of supported N–$TiO_2$ should be compared with an analysis of the support alone, as well as those observed for other supports. The main limitation or problem that can be found is when one or more of the typical analyses and spectrums of $TiO_2$ coincide with the support profiles, and relevant conclusions cannot be taken. Typical band peaks of Raman spectra for graphene can be detected at 1351 $cm^{-1}$ and 1593 $cm^{-1}$, but these peaks' intensity increased when higher amounts of graphene were applied for the preparation of N, S–$TiO_2$ graphene-supported catalysts [79]. On the other hand, Sacco et al. [121] immobilized N–$TiO_2$ over the polystyrene spheres, and verified that one polystyrene peak of Raman spectra was coincident with the peak of N–$TiO_2$. However, since the aim of these catalysts is the photodegradation of contaminants, their photocatalytic performance and the possibility of recovery and reuse should be considered the main target when comparing different catalytic materials. In this way, Brindha and Sivakumar [79] studied the photocatalytic degradation of Congo red, methylene blue, and reactive orange 16 using N, S co-doped $TiO_2$ supported on different amounts of graphene sheets (2.5%, 5%, 7.5%, and 10%). The most photoactive catalyst under visible light was the N, S–$TiO_2$ onto 5% of graphene, which was able to achieve decolorization rates of 93%, 94%, and 96% for Congo red (in 50 min), methylene blue (in 120 min), and reactive orange 16 (in 120 min), respectively. Moreover, after four cycles of reuse, the same efficiency regarding the decolorization of dyes was obtained, and no changes were detected regarding the crystalline phase [79], proving the stability of the catalyst. Still, results regarding the long-term operation of continuous reactors for wastewater treatment are lacking in the literature. Only in this way may reliable data be acquired regarding the stability of catalysts, which may boost their full-scale application. Another factor must be considered when comparing powder with supported catalysts: the mass of powder cannot be compared with the mass of the supported catalyst that is used. Instead, the best method of comparison is to consider the mass of the support as negligible, and just contemplate the amount of supported powder [79]. However, in the case of nanotubes rising from the Ti foil, the specific surface area or even the tube diameter and length can be compared [108,109].

Some studies can be found in the literature regarding supporting $TiO_2$ with other materials, such as pumice rock and zeolites [122]. The main reason for choosing these materials is their high porosity, which may correspond to a high surface area that can incorporate titanium dioxide nanoparticles [122]. This is important, since during the catalyst preparation, a significant reduction of the specific surface area may occur with the increase of calcination temperature. Huang et al. [122] verified an important reduction in the specific surface area with the increase of calcination temperatures from 110 to 500 °C, and consequently, a decrease in the decolorization rate when loading $TiO_2$ onto natural zeolite. These solids can present some disadvantages due to their leaching behavior, since this kind of material has metals and metal oxides in its composition [122,123]. In the photocatalytic processes, these characteristics can be very advantageous to the oxidative activity related to the degradation of contaminants. Otherwise, these processes normally promote rock leaching, which results in water contamination, since some of the metals that are leached can be toxic to aquatic organisms [124]. Still, these natural materials can be considered low-cost, and may reduce the costs associated with the supported catalysts' preparation.

## 8. N–$TiO_2$ Applications for the Removal of Emerging Contaminants

Normally, after the preparation and characterization of the catalyst, its photocatalytic activity is tested on the degradation of model compounds, such as for example phenols and dyes. However, when looking for applications related to real wastewater treatment, the use of a single contaminant may not be representative of the system behavior when applied to actual water treatment conditions. The meaning of the results obtained in terms of photocatalytic activity can be misrepresented when applied to real emerging contaminants. The performance of prepared catalysts should be evaluated against their undoped form and/or the best titanium dioxide catalyst. Considering the problematic of wastewater reclamation, the application of this methodology to remove emerging pollutants should be exploited, since these catalysts can present good activity under sunlight radiation, which is a very low-cost resource [125]. This would largely reduce the operating costs for water and wastewater treatment. New paradigms related to water recovery and reuse point out the need to seek suitable depuration strategies that are able to remove the so-called emerging contaminants from water, safeguarding ecosystems and human health. Among them, chemical compounds (such as pharmaceutical and personal care products) and biological species (such as bacteria, virus and protozoa) whose impact over public health is still not very well-defined ought to be highlighted. The precautionary principle imposes that their removal from water should be promoted. Thus, the application of N–$TiO_2$ catalysts for that purpose is now critically revised.

### *8.1. Chemical Emerging Contaminants Removal*

P25 is a commercial $TiO_2$ form that is found in the literature as active regarding the photocatalytic degradation of contaminants under sunlight or visible light radiation; thus, it should be used for comparative purposes when selecting an alternative photocatalyst. Some studies can be found about P25 doping with nitrogen. Authors have stated that doping can enhance P25 activity. However, improvement should also be measured in terms of both the preparation costs and the contaminants' degradation rate when using these novel catalysts versus undoped catalysts.

Mekprasart and Pecharapa [47] did not verify significant differences regarding the XRD patterns of P25 when doped with N. In the same way, rhodamine B photocatalytic decolorization under visible light after 60 min showed no significant differences between the application of P25 or N-doped P25. Still, the authors noted an increase in the decolorization kinetic constant from 0.051 to 0.105 $min^{-1}$ when changing the catalyst from P25 to N-doped P25 [47]. This difference regarding the reaction rate can be related to the higher initial dye absorption when N-doped P25 was used. However, in a general way, total decolorization was achieved at the same time for both catalysts. In this case, with the significant amount of nitrogen that was used (which was provided from ammonium hydrogen carbonate), it seems that there was an increase in the cost and time regarding the catalyst's preparation without a significant beneficial effect.

The degradation of 2-chlorophenol (2-CP) was tested using N–$TiO_2$ under visible light through a 150-W lamp applied together with 1 M of sodium nitrite working as a UV filter [21]. To study the photocatalytic oxidation of 2-CP, three different N precursors (diethanolamine, triethylamine, and urea) were used to prepare the N–$TiO_2$ by the sol–gel method [21]. The N–$TiO_2$ that was prepared using diethanolamine as the precursor presented the best 2-CP degradation compared to the other precursors. As described in Section 4, this was due to the smallest band gap, and the anatase crystal size was due to its better interstitial placement onto the $TiO_2$ lattice [21]. These authors observed almost double the kinetic rate for the catalyst prepared with diethanolamine compared to the other precursors that were used, and after 50 min of irradiation, it achieved 66% 2-CP removal. Moreover, the other catalysts that were prepared with the remaining dopant precursors presented higher efficiency on 2-CP removal than the Degussa P-25 ($TiO_2$). Ananpattarachai et al. [126] analyzed the effect of N–$TiO_2$ and N, C–$TiO_2$ produced by the sol–gel method using diethanolamine and triethanolamine as N and N, C precursors, respectively on the degradation of 2-chlorophenol (2-CP). The photocatalytic oxidation of 2-CP under visible light (420 to 700 nm for a 150-W lamp) occurred using one g/L of catalyst and pH 7. The best

result for 2-CP (initial concentration of 100 mg/L) degradation was obtained with the N,C–$TiO_2$ catalyst (95% of removal) while for N–$TiO_2$, only 70% of 2-CP removal was obtained after 30 min of irradiation.

Nolan et al. [13] studied the degradation of 4-chlorophenol (4-CP) using the N–$TiO_2$ prepared by the sol–gel method using 1,3-diaminopropane at different calcination temperatures from 400 to 800 °C. 4-CP degradation was obtained after two hours of irradiation. Parallelly, the authors analyzed the decolorization of methylene blue using a 60-W lamp, and concluded that the best performance was achieved for the catalyst prepared using 500 °C as the calcination temperature, where the anatase phase appears as unique. The increase of calcination temperature leads to a decrease in the decolorization kinetic rate, which increases again for the calcination temperature of 700 °C [13]. The authors noted that this increase was due to the appearance of rutile, which will reduce the band gap. However, for the degradation of 4-CP, the degradation profiles for these two calcination temperatures were not shown, prolonging the doubt of whether the presence of rutile can also enhance the N–$TiO_2$ photocatalytic activity of contaminant degradation.

Petala et al. [127] prepared N–$TiO_2$ by the sol–gel method under ammonia flow at calcination temperatures of 450 °C and 800 °C. Ethylparaben (EP) degradation was studied under simulated sunlight radiation using N–$TiO_2$ with different calcination temperatures, and the most active was the N–$TiO_2$ prepared for 600 °C. The efficacy could be attributed to the appearance of the rutile phase, which can help reduce the band gap. The degradation rate as a function of the catalyst load was also analyzed for 0.3 mg/L of EP, with the best result achieved for 750 mg/L. The increase from 100 mg/L to 750 mg/L enhanced the EP degradation rate, while for 1000 mg/L, the value was similar to the catalyst load of 750 mg/L.

Ramandi et al. [19] used a modified sol–gel method coupled with ultrasound irradiation to produce a tridoped C, N, S–$TiO_2$ to promote the degradation of diclofenac. The photocatalytic oxidation of diclofenac (25 mg/L) was performed using natural sunlight irradiation with a catalyst load of one g/L. Total degradation and mineralization were both achieved after 180 min of irradiation. The main factor responsible for the degradation efficiency was the oxidative species that were produced, such as superoxide and hydroxyl radicals, as proven by scavengers' usage.

Aba-Guevara et al. [128] verified the efficiency of Fe–N co-doped onto $TiO_2$ prepared by two different methods (sol–gel and microwaves) for amoxicillin, streptomycin, and diclofenac degradation under visible light. The main difference between these two preparation methods occurs during the hydrolysis, which for the sol–gel (SG) method happens at room temperature, and for the microwave (MW) method takes place under 100 W and 300 psi of pressure over 15 min. Photocatalytic oxidation occurs under a visible light lamp (23 W) with wavelength emissions above 400 nm, and each pharmaceutical compound was degraded in separate conditions at the initial concentration of 30 mg/L with a catalyst load of one g/L. After 240 min of irradiation, the amoxicillin degradation efficiencies were 58.6% (SG) and 46.1% (MW) at pH 3.5, while streptomycin obtained 49.7% (SG) and 39.9% (MW) removals at pH 8. Regarding diclofenac, the authors only noted 72.3% of removal after 300 min of irradiation for the MW method and pH 5. For this irradiation time, the authors also indicated for the MW method an increase of the degradation of amoxicillin and streptomycin, which reached about 69.2% and 72.3% for pH 3.5 and 8, respectively.

The degradation of 4-acetamidophenol was used to demonstrate the photocatalytic activity differences between N–$TiO_2$ prepared by conventional and ultrasonication sol–gel methods [129]. UV light (composed by UVB and UVA), aided by a N–$TiO_2$ concentration of 2 g/L, promoted 60% and 17% of 4-acetamidophenol (initial concentration of 50 mg/L) removal using the catalyst prepared by ultrasound and conventional methods, respectively [129]. Moreover, the authors concluded that the efficiency of the material prepared by the ultrasound method was related to the smaller particle sizes and higher surface area.

Pedrosa et al. [130] produced two different graphene oxides (based on the Hummers and Brodie methods), which through thermal treatment supported N–$TiO_2$. The effect of the N–$TiO_2$ support

on the photocatalytic performance of graphene oxide was evaluated regarding the degradation of diphenhydramine using UV/Vis radiation (wavelength 350 to 700 nm and photon flux of 140 W/m$^2$). After 60 min of irradiation and using 1 g/L of catalyst, it was possible to achieve about 65% and 70% diphenhydramine removal (initial concentration of 100 mg/L) for the Hummer and Brodie methods, respectively. Moreover, graphene oxides without N-doping presented the best performance regarding photocatalytic oxidation. For the N-doping process, the reduction of graphene oxide was needed through thermal treatment, which promoted a negative effect for photocatalysis [130].

N–$TiO_2$ produced by the sol–gel method using triethylamine as the N source was used through photocatalysis under blacklight lamps (which emit in the UVA range) to promote the degradation of a mixture of three herbicides (Picloram, Clopyralid and Triclopyr). The experimental conditions were: an initial concentration of each herbicide of 5 mg/L, a catalyst load of 0.5 g/L, and pH 4. The best result was achieved for the catalyst prepared with a Ti:N ratio of 1:1.6. At those conditions, 95% of picloram, 45% of clopyralid, and 90% of triclopyr were removed after 180 min of irradiation. Higher and lower ratios decreased the degradation rate [131].

Abramović et al. [132] produced N–$TiO_2$ by hydrolysis and verified its photocatalytic efficiency for the degradation of the following herbicides: RS-2-(4-chloro-o-tolyloxy), propionic acid (mecoprop), and (4-chloro-2-methylphenoxy) acetic acid (MCPA). Multiple ranges of catalyst loads from 1 g/L to 8 g/L with different radiations sources were used, and the initial concentration of each herbicide was 2.7 mM. A mercury lamp, which emits UVA and UVB rays, presented better results than a halogen lamp (visible light) or sunlight regarding the degradation of herbicides. On the other hand, the N–$TiO_2$ was more efficient than P25 for the degradation of herbicides under visible light, and for UV radiation, the opposite happens. A comparison between the prepared catalyst and P25 (a $TiO_2$ benchmark material) is essential in order to assess the feasibility of proposing a new catalytic material to the market. In this case, that N–$TiO_2$ is more efficient than P25 under visible light is quite relevant, since the use of less energetic radiation may reduce the treatment costs. Thus, this makes N–$TiO_2$ advantageous compared with P25.

Table 3 summarizes some of the literature results regarding the application of the N–$TiO_2$ catalyst for the removal of chemical emerging contaminants from water.

**Table 3.** Emerging contaminants degradation through photocatalytic oxidation.

| Ref. | Preparation Method | Pollutant | Conditions | Radiation | Results |
|---|---|---|---|---|---|
| [21] | Sol–gel method with diethanolamine, triethylamine, and urea as different N precursors | 2-CP (25 mg/L) | -Batch reactor (1.1 L)<br>-1 g/L of catalyst load; | Visible light (150-W lamp) | 66% of 2-CP removal after 50 min of irradiation (N source, diethanolamine; |
| [126] | Sol–gel method using diethanolamine and triethanolamine as N and N, C precursors | 2-CP (100 mg/L) | -1 g/L of catalyst load;<br>-30 min of irradiation; | Visible light (420–700 nm), 150 W | -N,C–$TiO_2$ catalyst, 95% of removal;<br>-N–$TiO_2$, only 70% of removal. |
| [13] | Sol–gel method | 4-CP (10 mg/L) | -Batch-stirred reactor;<br>-0.5 g/L of catalyst load;<br>-Calcination (500 °C) | Q-Sun solar chamber (average intensity 0.66 W/m$^2$); | Total degradation of 4-CP after two hours for calcination temperature of 500 °C. |
| [127] | Sol–gel method with flowing of ammonia | Ethylparaben (EP) (0.3 mg/L) | -Cylindrical glass reactor;<br>-Catalyst load 750 mg/L;<br>-Calcination temperature 600 °C;<br>-Different matrix conditions. | Solar simulator (100 W Xenon lamp) | -Total EP removal was achieved in 60 min with ultrapure water;<br>-Total EP removal was achieved in 60 min with wastewater;<br>-Toxicity of treated wastewater was higher than ultrapure water for the 60 min. |

**Table 3.** *Cont.*

| Ref. | Preparation Method | Pollutant | Conditions | Radiation | Results |
|---|---|---|---|---|---|
| [19] | Sol–gel method modified coupled with ultrasound irradiation | Diclofenac (25 mg/L) | -Water-jacketed reactor–Catalyst load 1g/L;<br>-C, S, N–$TiO_2$ used. | Natural sunlight irradiation; | C, S, N–$TiO_2$ allows total diclofenac degradation and total COD mineralization after 180 min of irradiation. |
| [128] | -Sol–gel method;<br>-Microwave method; | Amoxycilin, streptomycin, and diclofenac (30mg/L) | -Stirred reactor<br>-Fe,N–$TiO_2$ load 1g/L; | Visible light lamp (23 W) with wavelength emission above 400 nm; | -Amoxycilin removal: 58.6% (sol–gel, SG) and 46.1% (microwave, MW) at pH 3.5 (240 min of irradiation);<br>-Streptomycin removal: 49.7% (SG) and 39.9% (MW) at pH 8 (240 min of irradiation);<br>-Diclofenac removal: 72.3% of removal (MW) at pH 5 (after 300 min of irradiation). |
| [129] | Conventional and ultrasound sol–gel method | 4-acetamidophenol (50 mg/L) | -Stirred reactor with lamp placed axially.<br>-Catalyst load 1g/L; | UV light (composed by UVB: 280–315 nm and UVA: 315 to 400 nm); | -60% of removal for the catalyst prepared by ultrasound method;<br>-17% of removal for the catalyst prepared by conventional method. |
| [130] | -Hummers and Brodie method for graphene oxide.<br>-Thermal treatment in a furnace of $NH_3/N_2$ to N–$TiO_2$ reduced graphene oxide | Diphenhydramine (100 mg/L); | -Stirred glass reactor with gas bubbling;<br>-1g/L of catalyst load; | UV/Vis (wavelength 350 to 700 nm and photon flux of 140 $W/m^2$); | -65% of removal for Hummers graphene oxide N–$TiO_2$;<br>-70% of removal for Brodie graphene oxide N–$TiO_2$; |
| [131] | Sol–gel method using triethylamine as N source | -Three herbicides mixture (Picloram, Clopyralid, and Triclopyr);<br>-Initial concentration: 5 mg/L of each | -Catalyst load: 0.5 g/L;<br>-Ratio Ti:N—1: 1.6. | Blacklight lamps (UVA range); | -95% of picloram, 45% of clopyralid, and 90% of triclopyr were removed (at pH 4 and after 180 min of irradiation). |

### *8.2. Action on Some Pathogens*

Lee et al. [44] revealed that the N–$TiO_2$ prepared by the modified sol–gel method coupled with ultrasound irradiation presents a strong disinfection capacity over *Escherichia coli* and *Staphylococcus aureus* comparing to the undoped material. Two forms of N–$TiO_2$ were produced; one was irradiated with visible light for one hour, and the other one was without irradiation. The irradiated one revealed an increase in the surface hydrophilicity, as noted above. The bactericidal effect of irradiated N–$TiO_2$ was higher than the unirradiated one, since after one hour of visible light irradiation, no bacteria survival was verified, while for the unirradiated sample, a survival rate of 12.5% was still detected.

Rizzo et al. [8] concluded that the increase of the catalyst amount from the 0.025 to 0.2 g/L enhanced the *Escherichia coli* inactivation rate, which was probably due to the increased availability of active sites. However, the catalyst loads above 0.2 g/L until 0.5 g/L decreased the inactivation rate, which could be related with the increasing agglomeration of particles and/or due to the light scattering promoted by the higher N–$TiO_2$ loading [8]. Using a simulated sunlight radiation (250-W lamp) from an initial bacteria concentration ($10^7$ CFU/100mL), it was possible to achieve the complete disinfection after 60 min of irradiation with the N–$TiO_2$ load of 0.2 g/L.

Sacco et al. [121] used the solvent cast method to immobilize N–$TiO_2$ on polystyrene spheres, and evaluated the photocatalytic oxidation impact over *E. coli* provided from the real municipal wastewater after secondary settling. The packing catalyst was used (325 g) with a visible light radiation source from a strip of light-emitting diodes (LEDs) (81.6 W). The laboratory scale reactor was able to treat 500

mL of volume using a recirculation rate in the range of 6.3–74 mL/min. The authors also performed experiments under sunlight radiation, where the volume that was treated was 1.2 L, with a recirculation rate of 625 mL/min. Besides, 434 g of catalyst were used. In terms of results, inactivations of 92.6% and 87% of the initial *E. coli* concentration (300 CFU/mL) were achieved after 120 min of irradiation at the laboratory conditions and outdoor conditions, respectively.

Ata et al. [55] prepared N–$TiO_2$ by the sol–gel method supported on a polystyrene surface by the solvent-casting method to promote the inactivation of an antibiotic-resistant *E. coli* strain from the effluent provided from the biological process of a municipal wastewater treatment plant. The initial *E. coli* concentration was $10^5$ CFU/mL. The best result was achieved with 0.2 wt % of N–$TiO_2$ supported on the polystyrene support, since under visible light (emitting radiation between 400–800 nm), the inactivation of *E. coli* was about 97% in 30 min.

Table 4 summarizes some of the data concerning the application of N–$TiO_2$ catalysts for the removal of pathogens from water.

**Table 4.** Disinfection through photocatalytic oxidation.

| Ref. | Preparation Method | Pathogen | Conditions | Radiation | Results |
|---|---|---|---|---|---|
| [43] | Modified sol–gel method coupled with ultrasound irradiation | *E. coli* and *S. aureus* ($2 \times 10^5$ CFU/mL) | -25 mg/L of catalyst load; | Visible light (150-W Xe lamp) | -Surface hydrophilicity increases the antibacterial capacity;<br>-0% of survival bacteria after one hour of irradiation;<br>-12.5% of survival bacteria after one hour of irradiation for absence of surface hydrophilicity. |
| [8] | Hydrolysis method | *E. coli* ($10^7$ CFU/100 mL) | -0.025–0.5 g/L of catalyst;<br>-10 min of irradiation; | Simulated sunlight radiation (250-W lamp); | Higher inactivation rate $8.5 \times 10^5$ CFU/100 mL/min, for 0.2 g/L of catalyst load. |
| [121] | Hydrolysis method | *E. coli* (300 CFU/mL) | -325 g of catalyst and 500 mL of volume treated (lab conditions);<br>-434 g of catalyst and 1.2 L of volume treated (outdoor conditions); | Simulated sunlight radiation (LED, 81.6 W);<br>Natural sunlight (outdoor conditions); | -92.6% of *E. coli* inactivation after 120 min of irradiation (lab conditions);<br>-87% of *E. coli* inactivation after 120 min of irradiation (outdoor conditions). |
| [55] | Sol–gel method supported on polystyrene surface | *E. coli* ($10^5$ CFU/mL) | -0.2 wt.% of N–$TiO_2$ supported;<br>-diameter of polystyrene 8.5 cm;<br>-Real wastewater; | Visible light (400 nm and 800 nm). | -inactivation of *E. coli* was about 97% after 30 min of irradiation. |

The improvement of the photocatalytic oxidation that was verified through using this kind of catalyst for the degradation of chemical and biological contaminants is usually related to the availability of reactive oxygen species due to the band-gap reduction. The production of radical species such as hydroxyl and superoxide may enhance decontamination and disinfection.

## 9. Conclusions and Future Perspectives

N–$TiO_2$ can be prepared in different ways; its advantages are related the production rate, and its disadvantages are related to the energetic costs and the requirement of special equipment. There are other production technologies with slower production rates, but that also have lower operating costs and do not require special equipment. The production methods can be modified in order to achieve a material with the best photocatalytic performance. In fact, the preparation procedure was shown to have a large influence on the final catalyst properties. The selection of the best preparation methodology must bear in mind the obtained material properties (particularly photoactivity under

visible/sunlight radiation), including its stability as well as the costs associated with its production. The preparation procedure must not have prohibitive implementation/operating costs when scaled-up to the industrial level. Among the described methodologies, the sol–gel method seems to be the easiest to implement, and it is flexible enough to change the obtaining catalyst properties by manipulating the operating conditions. Still, this method requires more chemicals, as well as a calcination step.

Some characteristics such as surface hydrophilicity and the type of crystalline phases can be helpful for enhancing the photocatalytic activity of the material. Thus, the preparation method should be designed to enhance those features. Still, the way that N is incorporated in $TiO_2$ is controversial, and seems to depend on the preparation procedure. It seems hard to rely on the data obtained from a single characterization analysis to draw any conclusions regarding the effectiveness of the preparation procedure. Rather, several analytical techniques should be joined together to characterize the catalysts. Besides, the selection of a suitable catalyst should consider the screening of several materials and compare their activity and stability on the photocatalytic degradation of the contaminants under visible/sunlight radiation.

Co-doping N–$TiO_2$ can improve its photocatalytic activity under visible or sunlight radiation, since the presence of the co-dopant can further reduce the catalyst band gap. Thus, some co-dopants such as F, Ce, and Pt can enhance the degradation of contaminants during photocatalytic oxidation. The selection of the best catalyst must consider its activity, stability, and production costs, so that a cost-effective water treatment process can be obtained.

While most of the studies involving N–$TiO_2$ consider it in the powder form, this is not the best way to operate a photocatalytic reactor under real water treatment conditions. Thus, supports have been exploited to reduce the cost of their real application, since this way, the catalysts could be used in a continuous reactor without requiring a posterior separation process. Alternatively, N–$TiO_2$ nanotubes can grow from Ti foils' support. The design of a reactor to work with supported N–$TiO_2$ is a challenge, since mass-transfer limitations and lower effective light absorption by the catalyst will reduce treatment efficiency. Still, research efforts must be put into action in order to reach suitable solutions to boost the wide real-scale application of this treatment technology. Thus, more studies considering the emerging degradation of contaminants using supported N–$TiO_2$ should be performed to ensure that the decrease in the catalyst activity resulting from the support will not make the process unviable. To attest to the economic viability of supported N–$TiO_2$ applications involving real wastewaters in pilot, solar reactors are required. This way, the effects of factors such as hydrodynamics, reactor dimensions, and the type of support could be analyzed. On the other hand, the reuse of these supported catalysts must be evaluated in order to attest their stability regarding water treatment conditions. Another important point is related to P25, which is a benchmark photocatalyst. Thus, the efficiency of the catalysts that are developed must be compared with this material to verify whether the new catalysts are truly an alternative.

The selection of a suitable treatment for emerging contaminants removal must involve the screening of several technologies [133,134], and must consider their economic aspects.

**Author Contributions:** Conceptualization, J.G.; R.C.M., data curation, J.G.; E.D.; J.L.; writing—original draft preparation, J.G., E.D. writing—review and editing, R.M.Q.-F. and R.C.M.; supervision, R.M.Q.-F. and R.C.M.; project administration, R.C.M.; funding acquisition, R.C.M.

**Funding:** João Gomes and Rui C. Martins gratefully acknowledge Fundação para a Ciência e Tecnologia by the financial support under IFCT2014 programme (IF/00215/2014) with financing from the European Social Fund and the Human Potential Operational Programme.

**Conflicts of Interest:** The authors declare no conflict of interest.

## References


1. Gaya, U.I.; Abdullah, A.H. Heterogeneous photocatalytic degradation of organic contaminants over titanium dioxide: A review of fundamentals, progress and problems. *J. Photochem. Photobiol. C Photochem. Rev.* **2008**, *9*, 1–12. [CrossRef]
2. Chong, M.; Jin, B.; Chow, C.W.; Saint, C. Recent developments in photocatalytic water treatment technology: A review. *Water Res.* **2010**, *44*, 2997–3027. [CrossRef] [PubMed]
3. Pelaez, M.; Nolan, N.T.; Pillai, S.C.; Seery, M.K.; Falaras, P.; Kontos, A.G.; Dunlop, P.S.; Hamilton, J.W.; Byrne, J.A.; O'Shea, K.; et al. A review on the visible light active titanium dioxide photocatalysts for environmental applications. *Appl. Catal. B Environ.* **2012**, *125*, 331–349. [CrossRef]
4. Yuan, J.; Chen, M.; Shi, J.; Shangguan, W. Preparations and photocatalytic hydrogen evolution of N-doped $TiO_2$ from urea and titanium tetrachloride. *Int. J. Hydrog. Energy* **2006**, *31*, 1326–1331. [CrossRef]
5. Fujishima, A.; Zhang, X.; Tryk, D.A. $TiO_2$ photocatalysis and related surface phenomena. *Surf. Sci. Rep.* **2008**, *63*, 515–582. [CrossRef]
6. Sun, X.; Liu, H.; Dong, J.; Wei, J.; Zhang, Y. Preparation and characterization of Ce/N-Co-doped $TiO_2$ particles for production of $H_2$ by photocatalytic splitting water under visible light. *Catal. Lett.* **2010**, *135*, 219–225. [CrossRef]
7. Antony, R.P.; Mathews, T.; Ajikumar, P.K.; Krishna, D.N.; Dash, S.; Tyagi, A.K. Electrochemically synthesized visible light absorbing vertically aligned N-doped $TiO_2$ nanotube array films. *Mater. Res. Bull.* **2012**, *47*, 4491–4497. [CrossRef]
8. Rizzo, L.; Sannino, D.; Vaiano, V.; Sacco, O.; Scarpa, A.; Pietrogiacomi, D. Effect of solar simulated N-doped $TiO_2$ photocatalysis on the inactivation and antibiotic resistance of an *E. coli* strain in biologicallytreated urban wastewater. *Appl. Catal. B Environ.* **2014**, *144*, 369–378. [CrossRef]
9. Gomes, J.; Costa, R.; Quinta-Ferreira, R.M.; Martins, R.C. Application of ozonation for pharmaceuticals and personal care products removal from water. *Sci. Total Environ.* **2017**, *586*, 265–283. [CrossRef]
10. Khaki, M.R.D.; Shafeeyan, M.S.; Raman, A.A.A.; Daud, W.M.A.W. Application of doped photocatalysts for organic pollutant degradation—A review. *J. Environ. Manag.* **2017**, *198*, 78–94. [CrossRef]
11. Molins-Delgado, D.; Díaz-Cruz, M.S.; Barceló, D. Ecological risk assessment associated to the removal of endocrine-disrupting parabens and benzophenone-4 in wastewater treatment. *J. Hazard. Mater.* **2016**, *310*, 143–151. [CrossRef] [PubMed]
12. Henderson, M.A. A surface science perspective on $TiO_2$ photocatalysis. *Surf. Sci. Rep.* **2011**, *66*, 185–297. [CrossRef]
13. Nolan, N.T.; Synnott, D.W.; Seery, M.K.; Hinder, S.J.; Wassenhoven, A.V.; Pillai, S.C. Effect of N-doping on the photocatalytic activity of sol–gel $TiO_2$. *J. Hazard. Mater.* **2012**, *211–212*, 88–94. [CrossRef] [PubMed]
14. Gomes, J.; Lopes, A.; Gmurek, M.; Quinta-Ferreira, R.M.; Martins, R.C. Study of the influence of the matrix characteristics over the photocatalytic ozonation of parabens using Ag-$TiO_2$. *Sci. Total Enviorn.* **2019**, *646*, 1468–1477. [CrossRef] [PubMed]
15. Barkul, R.P.; Koli, V.B.; Shewale, V.B.; Patil, M.K.; Delekar, S.D. Visible active nanocrystalline N-doped anatase $TiO_2$ particles for photocatalytic mineralization studies. *Mater. Chem. Phys.* **2016**, *173*, 42–51. [CrossRef]
16. Zheng, Z.; Huang, B.B.; Qin, X.Y.; Zhang, X.Y.; Dai, Y.; Whangbo, M.H. Facile in situ synthesis of visible-light plasmonic photocatalysts M@$TiO_2$ (M = Au, Pt, Ag) and evaluation of their photocatalytic oxidation of benzene to phenol. *J. Mater. Chem.* **2011**, *21*, 9079–9087. [CrossRef]
17. Wang, P.; Huang, B.; Dai, Y.; Whangbo, M. Plasmonic photocatalysts: Harvesting visible light with noble metal nanoparticles. *Phys. Chem. Chem. Phys.* **2012**, *14*, 9813–9825. [CrossRef]
18. Gomes, J.; Leal, I.; Bednarczyk, K.; Gmurek, M.; Stelmachowski, M.; Zaleska-Medynska, A.; Bastos, F.C.; Quinta-Ferreira, M.E.; Costa, R.; Quinta-Ferreira, R.M.; et al. Detoxification of Parabens Using UV-A enhanced by Noble Metals—$TiO_2$ Supported Catalysts. *J. Environ. Chem. Eng.* **2017**, *5*, 3065–3074. [CrossRef]
19. Ramandi, S.; Entezari, M.H.; Ghows, N. Sono-synthesis of solar light responsive S-N-C-tri doped $TiO_2$ photo-catalyst under optimized conditions for degradation and mineralization of Diclofenac. *Ultrason. Sonochem.* **2017**, *38*, 234–245. [CrossRef]
20. Irie, H.; Watanabe, Y.; Hashimoto, K. Nitrogen-concentration dependence on photocatalytic activity of $TiO_2$-x Nx Powders. *J. Phys. Chem. B* **2003**, *107*, 5483–5486. [CrossRef]

21. Ananpattarachai, J.; Kajitvichyanukul, P.; Seraphin, S. Visible light absorption ability and photocatalytic oxidation activity of various interstitial N-doped $TiO_2$ prepared from different nitrogen dopants. *J. Hazard. Mater.* **2009**, *168*, 253–261. [CrossRef] [PubMed]
22. Asahi, R.; Morikawa, T.; Irie, H.; Ohwaki, T. Nitrogen-Doped Titanium Dioxide as Visible-Light-Sensitive Photocatalyst: Designs, Developments, and Prospects. *Chem. Rev.* **2014**, *114*, 9824–9852. [CrossRef] [PubMed]
23. Valentin, C.D.; Pacchioni, G.; Selloni, A. Origin of the different photoactivity ofN-doped anatase and rutile $TiO_2$. *Phys. Rev. B Condens. Matter Mater. Phys.* **2004**, *70*, 1–4. [CrossRef]
24. Selvaraj, A.; Sivakumar, S.; Ramasamy, A.K.; Balasubramanian, V. Photocatalytic degradation of triazine dyes over N-doped $TiO_2$ in solar radiation. *Res. Chem. Intermed.* **2013**, *39*, 2287–2302. [CrossRef]
25. Ghicov, A.; Macak, J.M.; Tsuchiya, H.; Kunze, J.; Haeublein, V.; Frey, L.; Schmuki, P. Ion implantation and annealing for an efficient N-doping of $TiO_2$ nanotubes. *Nano Lett.* **2006**, *6*, 1080–1082. [CrossRef]
26. Asahi, R.; Morikawa, T.; Ohwaki, T.; Aoki, K.; Taga, Y. Visible-light photocatalysis in nitrogen-doped titanium oxides. *Science* **2001**, *293*, 269–271. [CrossRef] [PubMed]
27. Nasirian, M.; Mehrvar, M. Photocatalytic degradation of aqueous Methyl Orange usingnitrogen-doped $TiO_2$ photocatalyst prepared by novelmethod of ultraviolet-assisted thermal synthesis. *J. Environ. Sci.* **2018**, *66*, 81–93. [CrossRef]
28. Chen, C.; Bai, H.; Chang, S.M.; Chang, C.; Den, W. Preparation of N-doped $TiO_2$ photocatalyst byatmospheric pressure plasmaprocess for VOCs decomposition under UV and visible light sources. *J. Nanopart. Res.* **2007**, *9*, 365–375. [CrossRef]
29. Burda, C.; Lou, Y.; Chen, X.; Samia, A.C.S.; Stout, J.; Gole, J.L. Enhanced Nitrogen Doping in $TiO_2$Nanoparticles. *Nano Lett.* **2003**, *3*, 1049–1051. [CrossRef]
30. Peng, F.; Cai, L.; Huang, H.; Yu, H.; Wang, H. Preparation of nitrogen-doped titanium dioxide with visible-light photocatalytic activity using a facile hydrothermal method. *J. Phys. Chem. Solids* **2008**, *69*, 1657–1664. [CrossRef]
31. Hu, S.; Wang, A.; Li, X.; Lowe, H. Hydrothermal synthesis of well-dispersed ultrafine N-doped $TiO_2$ nanoparticles with enhanced photocatalytic activity under visible light. *J. Phys. Chem. Solids* **2010**, *71*, 156–162. [CrossRef]
32. Li, Z.; Zhu, Y.; Pang, F.; Liu, H.; Gao, X.; Ou, W.; Liu, J.; Wang, X.; Cheng, X.; Zhang, Y. Synthesis of N doped and N, S co-doped 3D $TiO_2$ hollow spheres with enhanced photocatalytic efficiency under nature sunlight. *Ceram. Int.* **2015**, *41*, 10063–10069. [CrossRef]
33. Morikawa, T.; Asahi, R.; Ohwaki, T.; Aoki, K.; Taga, Y. Band-gap narrowing of titanium dioxide by nitrogen doping. *Jpn. J. Appl. Phys.* **2001**, *40*, 1561–1563. [CrossRef]
34. Zhu, L.; Xie, J.; Cui, X.; Shen, J.; Yang, X.; Zhang, Z. Photoelectrochemical and optical propertiesof N-doped $TiO_2$ thin films preparedby oxidation of sputtered TiNx films. *Vaccum* **2010**, *84*, 797–802. [CrossRef]
35. Zhou, X.; Peng, F.; Wang, H.; Yu, H.; Yang, J. Preparation of nitrogen doped $TiO_2$ photocatalyst by oxidation of titaniumnitride with $H_2O_2$. *Mater. Res. Bull.* **2011**, *46*, 840–844. [CrossRef]
36. Sathish, M.; Viswanathan, B.; Viswanathan, R.P.; Gopinath, C.S. Synthesis, characterization, electronic structure and photocatalytic activity of nitrogen-doped $TiO_2$ nanocatalyst. *Chem. Mater.* **2005**, *17*, 6349–6353. [CrossRef]
37. Huang, L.; Fu, W.; Fu, X.; Zong, B.; Liu, H.; Bala, H.; Wang, X.; Sun, G.; Cao, J.; Zhang, Z. Facile and large-scale preparation of N doped $TiO_2$ photocatalyst withhigh visible light photocatalytic activity. *Mater. Lett.* **2017**, *209*, 585–588. [CrossRef]
38. Sacco, O.; Stoller, M.; Vaiano, V.; Ciambelli, P.; Chianese, A.; Sannino, D. Photocatalytic Degradation of Organic Dyes underVisible Light on N-Doped $TiO_2$ Photocatalysts. *Int. J. Photoenergy* **2012**, *2012*, 626759. [CrossRef]
39. Nosaka, Y.; Matsushita, M.; Nishino, J.; Nosaka, A.Y. Nitrogen-doped titanium dioxide photocatalysts for visible responseprepared by using organic compounds. *Sci. Technol. Adv. Mater.* **2005**, *6*, 143–148.
40. Hu, L.; Wang, J.; Zhang, J.; Zangh, Q.; Liu, Z. An N-doped anatase/rutile $TiO_2$ hybrid from low-temperature direct nitridization: Enhanced photoactivity under UV-/visible-light. *RSC Adv.* **2014**, *4*, 420–427. [CrossRef]
41. Devi, L.G.; Kavitha, R. Review on modified N–$TiO_2$ for green energy applications under UV/visible light: Selected results and reaction mechanisms. *RSC Adv.* **2014**, *4*, 28265–28299. [CrossRef]
42. Zhu, Y.-J.; Chen, F. Microwave-assisted preparation ofinorganic nanostructures in liquid phase. *Chem. Rev.* **2014**, *114*, 6462–6555. [CrossRef]

43. Akpan, U.G.; Hameed, B.H. The advancements in sol-gel method of doped-$TiO_2$ photocatalysts. *Appl. Catal. A Gen.* **2010**, *375*, 1–11. [CrossRef]
44. Lee, H.U.; Lee, S.C.; Choi, S.; Son, B.; Lee, S.M.; Kim, H.J.; Lee, J. Efficient visible-light induced photocatalyst on nanoporous nitrogen-doped titanium dioxide catalysts. *Chem. Eng. J.* **2013**, *228*, 756–764. [CrossRef]
45. Guo, Q.; Zhang, Z.; Ma, X.; Jing, K.; Shen, M.; Yu, N.; Tang, J.; Dionysiou, D.D. Preparation of N,F-co-doped $TiO_2$ nanoparticles by three different methods and comparison of visible-light photocatalytic performances. *Sep. Purif. Technol.* **2017**, *175*, 305–313. [CrossRef]
46. Galenda, A.; Crociani, L.; El Habra, N.; Favaro, M.; Natile, M.M.; Rossetto, G. Effect of reaction conditions on methyl red degradation mediated byboron and nitrogen doped $TiO_2$. *Appl. Surf. Sci.* **2014**, *314*, 919–930. [CrossRef]
47. Mekprasart, W.; Pecharapa, W. Synthesis and characterization of nitrogen-doped $TiO_2$ and itsphotocatalytic activity enhancement under visible light. *Energy Procedia* **2011**, *9*, 509–514. [CrossRef]
48. Zaleska, A. Doped $TiO_2$-Review. *Rec. Pat. Eng.* **2008**, *2*, 157–164. [CrossRef]
49. Wang, X.C.; Yu, J.C.; Chen, Y.L.; Wu, L.; Fu, X.Z. $ZrO_2$-modified mesoporous nanocrystalline $TiO_2$-xNx as efficient visible light photocatalysts. *Environ. Sci. Technol.* **2006**, *40*, 2369–2374. [CrossRef]
50. Valentin, C.D.; Finazzi, E.; Pacchioni, G.; Selloni, A.; Livraghi, S.; Paganini, M.C.; Giamello, E. N-doped $TiO_2$: Theory and experiment. *Chem. Phys.* **2007**, *339*, 44–56. [CrossRef]
51. Viswanathan, B.; Krishnamurthy, K.R. Nitrogen incorporation in $TiO_2$: Does it make a visible light photo-active material? *Int. J. Photoenergy* **2012**, *2012*, 269654. [CrossRef]
52. Herrmann, J.M. Photocatalysis fundamentals revisited to avoid several miscon-ceptions. *Appl. Catal. B Environ.* **2010**, *99*, 461–468. [CrossRef]
53. Ohtani, B.; Ogawa, Y.; Nishimoto, S.I. Photocatalytic activity of amorphous anatase mixture of titanium (IV) oxide particles suspended in aqueous solutions. *J. Phys. Chem. B* **1997**, *101*, 3746–3752. [CrossRef]
54. Kaur, K.; Singh, C.V. Amorphous $TiO_2$ as a photocatalyst for hydrogen production: A DFT study of structural and electronic properties. *Energy Procedia* **2012**, *29*, 291–299. [CrossRef]
55. Ata, R.; Sacco, O.; Vaiano, V.; Rizzo, L.; Tore, G.Y.; Sannino, D. Visible light active N-doped $TiO_2$ immobilized on polystyrene as efficient system for wastewater treatment. *J. Phys. Chem. A Chem.* **2017**, *348*, 255–262. [CrossRef]
56. Yan, M.; Chen, F.; Zhang, J.; Anpo, M. Preparation of controllable crystalline titania and study on the photocatalytic properties. *J. Phys. Chem. B* **2005**, *109*, 8673–8678. [CrossRef] [PubMed]
57. Katoueizadeh, E.; Zebarjad, S.M.; Janghorban, K. Optimization of synthesis conditions of N-doped $TiO_2$ nanoparticles using Taguchi robust design. *Mater. Chem. Phys.* **2017**, *201*, 69–77. [CrossRef]
58. Yang, G.; Jiang, Z.; Shi, H.; Xiao, T.; Yan, Z. Preparation of highly visible-light active N-doped $TiO_2$ photocatalyst. *J. Mater. Chem.* **2010**, *20*, 5301–5309. [CrossRef]
59. Syafiuddin, A.; Hadibarata, T.; Zon, N.F. Salmiati, Characterization of Titanium Dioxide Doped with Nitrogen and Sulfur and its Photocatalytic Appraisal for Degradation of Phenol and Methylene Blue. *J. Chin. Chem. Soc.* **2017**, *64*, 1333–1339. [CrossRef]
60. Huo, Y.N.; Jin, Y.; Zhu, J.; Li, H.X. Highly active $TiO_2-x-yNxFy$ visible photocatalyst prepared under supercritical conditions in $NH_4F/EtOH$ fluid. *Appl. Catal. B* **2009**, *89*, 543–550. [CrossRef]
61. Etacheri, V.; Seery, M.; Hinder, S.; Pillai, S. Highly Visible Light Active $TiO_2$-xNx Heterojunction Photocatalysts. *Chem. Mater.* **2010**, *22*, 3843–3853. [CrossRef]
62. Wang, H.; Yang, X.; Xiong, W.; Zhang, Z. Photocatalytic reduction of nitroarenes to azo compounds over N-doped $TiO_2$: Relationship between catalysts and chemical reactivity. *Res. Chem. Intermed.* **2015**, *41*, 3981–3997. [CrossRef]
63. Jackson, A.W.; Shebanova, O.; Hector, A.L.; McMillan, P.F. Amorphous and nanocrystalline titanium nitride and carbonitride materials obtained by solution phase ammonolysis of $Ti(NMe_2)_4$. *Solid State Chem.* **2006**, *179*, 1383–1393.
64. Li, H.; Hao, Y.; Lu, H.; Liang, L.; Wang, Y.; Qiu, J.; Shi, X.; Wang, Y.; Yao, J. A systematic study on visible-light N-doped $TiO_2$photocatalystobtained from ethylenediamine by sol–gel method. *Appl. Surf. Sci.* **2015**, *344*, 112–118. [CrossRef]
65. Ou, H.H.; Lo, S.L.; Liao, C.H. N-doped $TiO_2$ prepared from microwave-assisted titanate nanotubes ($NaxH_2$-$xTi_3O_7$): The effect of microwave irradiation during TNT synthesis on the visible light photoactivity of N-doped $TiO_2$. *J. Phys. Chem. C* **2011**, *115*, 4000–4007. [CrossRef]

66. Mrowetz, M.; Balcerski, W.; Colussi, A.J.; Hoffmann, M.R. Oxidative power of nitrogen-doped $TiO_2$ photocatalysts under visible illumination. *J. Phys. Chem. B* **2004**, *108*, 17269–17273. [CrossRef]
67. Zhou, Y.; Liu, Y.; Liu, P.; Zhang, W.; Xing, M.; Zhang, J. A facile approach to further improve the substitution of nitrogen into reduced $TiO_2$-x with an enhanced photocatalytic activity. *Appl. Catal. B Environ.* **2015**, *170–171*, 66–73. [CrossRef]
68. O'Regen, B.; Gratzel, M. A low cost high efficiency solar cell based on dye sensitized colloidal $TiO_2$ films. *Nature* **1991**, *353*, 737–740.
69. Pérez, E.; Torres, M.F.; Morales, G.; Murgia, V.; Sham, E. Synthesis of N-$TiO_2$ Effect of the Concentration of Nitrogen in the Band Gap. *Procedia Mater. Sci.* **2015**, *8*, 649–655. [CrossRef]
70. Chainarong, S.; Sikong, L.; Pavasupree, S.; Niyomwas, S. Synthesis and Characterization of Nitrogen-doped $TiO_2$ Nanomaterials for Photocatalytic Activities under Visible Light. *Energy Procedia* **2011**, *9*, 418–427. [CrossRef]
71. Zhang, J.; Li, M.; Feng, Z.; Chen, J.; Li, C. UV Raman Spectroscopic Study on $TiO_2$. I. Phase Transformation at the Surface and in the Bulk. *J. Phys. Chem. B* **2006**, *110*, 927–935. [CrossRef]
72. Cong, Y.; Zhang, J.; Chen, F.; Anpo, M. Synthesis and characterization of nitrogen-doped $TiO_2$ nanophotocatalyst with high visible light activity. *J. Phys. Chem. C* **2007**, *111*, 6976–6982. [CrossRef]
73. Bersani, D.; Lottici, P.P.; Ding, X.Z. Phonon confinement effects in the Raman scattering by $TiO_2$ nanocrystals. *Appl. Phys. Lett.* **1998**, *72*, 73–75. [CrossRef]
74. Gurkan, Y.Y.; Turkten, N.; Hatipogluand, A.; Cinar, Z. Photocatalytic degradation of cefazolin over N-doped $TiO_2$ under UV and sunlight irradiation: Prediction of the reaction paths via conceptual DFT. *Chem. Eng. J.* **2012**, *184*, 113–124. [CrossRef]
75. Kassahun, S.K.; Kiflie, Z.; Shin, D.W.; Park, S.S.; Jung, W.Y.; Chung, Y.R. Optimization of sol-gel synthesis parameters in the preparation of N-doped $TiO_2$ using surface response methodology. *J. Sol-Gel Sci. Technol.* **2017**, *82*, 322–334. [CrossRef]
76. Nolan, N.T.; Seery, M.K.; Hinder, S.J.; Healy, L.F.; Pillai, S.C. A systematic study of the effect of silver on the chelation of formic acid to a titanium precursor and the resulting effect on the anatase-to-rutile transformation of $TiO_2$. *J. Phys. Chem. C* **2010**, *114*, 13026. [CrossRef]
77. Hanaor, D.A.H.; Sorrell, C.C. Review of the anatase to rutile phase transformation. *J. Mater. Sci.* **2011**, *46*, 855–874. [CrossRef]
78. Umebayashi, T.; Yamaki, T.; Tanaka, S.; Asai, K. Visible-Light-Induced Degradation of Methylene Blue on S-Doped $TiO_2$. *Chem. Lett.* **2003**, *32*, 330–331. [CrossRef]
79. Brindha, A.; Sivakumar, T. Visible active N,S co-doped $TiO_2$/graphene photocatalysts for the degradation of hazardous dyes. *J. Photochem. Phtotobiol. A Chem.* **2017**, *340*, 146–156. [CrossRef]
80. Kumar, N.; Maitra, U.; Hedge, V.I.; Waghmare, U.V.; Sundaresan, A.; Rao, C.N.R. Synthesis, Characterization, photocatalysis, and varied properties of $TiO_2$ cosubstituted with nitrogen and fluorine. *Inorg. Chem.* **2013**, *52*, 10512–10519. [CrossRef]
81. Yang, G.; Wang, T.; Yang, B.; Yan, Z.; Ding, S.; Xiao, T. Enhanced visible-light activity of F-N co-doped $TiO_2$ nanocrystals via nonmetal impurity, $Ti^{3+}$ ions and oxygen vacancies. *Appl. Surf. Sci.* **2013**, *287*, 135–142. [CrossRef]
82. Zhang, G.; Zhang, Y.C.; NAdagoud, M.; Han, C.; O'Shead, K.; El-Sheikhe, S.M.; Ismaile, A.A.; Dionysiou, D.D. Visible light-sensitized S, N, and C co-doped polimorphic $TiO_2$ for photocatalytic destruction of microcystin-LR. *Appl. Catal. B Environ.* **2014**, *144*, 614–621. [CrossRef]
83. Shen, X.Z.; Guo, J.; Liu, Z.C.; Xie, S.M. Visible-light-driven titania photocatalyst co-doped with nitrogen and ferrum. *Appl. Surf. Sci.* **2008**, *254*, 4726–4731. [CrossRef]
84. Nkambule, T.I.; Kuvarega, A.T.; Krause, R.W.M.; Haarhoff, J.; Mamba, B.B. Synthesis and characterisation of Pd-modified N-doped $TiO_2$ for photocatalytic degradation of natural organic matter (NOM) fractions. *Enviorn. Pollut.* **2012**, *19*, 4120–4132. [CrossRef]
85. Sharotri, N.; Sud, D. A greener approach to synthesize visible light responsive nanoporous S-doped $TiO_2$ with enhanced photocatalytic activity. *New J. Chem.* **2015**, *39*, 2217–2223. [CrossRef]
86. Ingo, G.M.; Paparazzo, E.; Bagnarelli, O.; Zacchetti, N. XPS studies on cerium, zirconium and yttrium valence states in plasma-sprayed coatings. *Surf. Interface Anal.* **1990**, *16*, 515–519. [CrossRef]

87. Choi, H.; Antoniou, M.G.; Pelaez, M.; De La Cruz, A.A.; Shoemaker, J.A.; Dionysiou, D.D. Mesoporous Nitrogen-Doped $TiO_2$ for the Photocatalytic Destruction of the Cyanobacterial Toxin Microcystin-LR under Visible Light Irradiation. *Environ. Sci. Technol.* **2007**, *41*, 7530–7535. [CrossRef]
88. Sakthivel, S.; Kisch, H. Photocatalytic and photoelectrochemical properties of nitrogen-doped titanium dioxide. *ChemPhysChem* **2003**, *4*, 487. [CrossRef]
89. Kryukova, G.N.; Zenkovets, G.A.; Shutilov, A.A.; Wilde, M.; Gunther, K.; Fassler, D.; Richter, K. Structural peculiarities of $TiO_2$ and Pt/$TiO_2$ catalysts for the photocatalytic oxidation of aqueous solution of acid Orange 7 Dye upon ultraviolet light. *Appl. Catal. B Environ.* **2007**, *71*, 169–176. [CrossRef]
90. Zielinska-Jurek, A.; Wysocka, I.; Janczarek, M.; Stampor, W.; Hupka, J. Preparation and characterization of Pt–N/$TiO_2$ photocatalysts and their efficiency in degradation of recalcitrant chemicals. *Sep. Purif. Technol.* **2015**, *156*, 369–378. [CrossRef]
91. Diwald, O.; Thompson, T.L.; Zubkov, T.; Walck, S.D.; Yates, J.T. Photochemical activity of nitrogen-doped rutile $TiO_2$(110) in visible light. *J. Phys. Chem. B* **2004**, *108*, 6004–6008. [CrossRef]
92. Teh, C.Y.; Wu, T.Y.; Juan, J.C. Facile sonochemical synthesis of N,Cl-co-doped $TiO_2$: Synthesis effects, mechanism and photocatalytic performance. *Catal. Today* **2015**, *256*, 365–374. [CrossRef]
93. Brus, L. Electronic wave functions in semiconductor clusters: Experiment and theory. *J. Phys. Chem.* **1986**, *90*, 2555–2560. [CrossRef]
94. Zhang, Z.B.; Wang, C.C.; Zakaria, R.; Ying, J.Y. Role of particle size in nanocrystalline $TiO_2$-based photocatalysts. *J. Phys. Chem. B* **1998**, *102*, 10871–10878. [CrossRef]
95. González-Reyes, L.; Hernández-Pérez, I.; Díaz-Barriga Arceo, L.; Dorantes-Rosales, H.; Arce-Estrada, E.; Suárez-Parra, R.; Cruz-Rivera, J. Temperature effects during Ostwald ripening on structural and bandgap properties of $TiO_2$ nanoparticles prepared by sonochemical synthesis. *J. Mater. Sci. Eng. B* **2010**, *175*, 9–13. [CrossRef]
96. Prasad, K.; Pinjari, D.V.; Pandit, A.B.; Mhaske, S.T. Phase transformation of nanostructured titanium dioxide from anatase-to-rutile via combined ultrasound assisted sol–gel technique. *Ultrason. Sonochem.* **2010**, *17*, 409–415. [CrossRef]
97. Shchukin, D.G.; Skorb, E.; Belova, V.; Möhwald, H. Ultrasonic cavitation at solid surfaces. *Adv. Mater.* **2011**, *23*, 1922–1934. [CrossRef]
98. Lee, H.U.; Ahn, K.; Jeong, S.Y.; Cho, C.R.; Kim, J.P.; Bae, J.S.; Kim, H.G.; Kwon, S.H.; Lee, H.W. Enhanced photocatalytic activity of $TiO_2$ nanobarbed fibers treated with atmospheric pressure plasma using $O_2$ gas. *Appl. Phys. Lett.* **2010**, *97*, 223111. [CrossRef]
99. Rengifo-Herrera, J.A.; Pierzchala, K.; Sienkiewicz, A.; Forro, L.; Kiwi, J.; Pulgarin, C. Abatement of organics and Escherichia coli by N, S co-doped $TiO_2$ under UV and visible light. Implications of the formation of singlet oxygen ($^1O_2$) under visible light. *Appl. Catal. B Environ.* **2009**, *88*, 398–406. [CrossRef]
100. Vaiano, V.; Sacco, O.; Sannino, D.; Navarra, W.; Daniel, C.; Venditto, V. Influence of aggregate size on photoactivity of N-doped $TiO_2$ particles in aqueous suspensions under visible light irradiation. *J. Photochem. Photobiol. A Chem.* **2017**, *336*, 191–197. [CrossRef]
101. Othman, S.H.; Rashid, S.A.; Ghazi, T.I.M.; Abdullah, N. Dispersion and stabilization of photocatalytic $TiO_2$ nanoparticles in aqueous suspension for coatings applications. *J. Nanomater.* **2012**, *2012*, 718214. [CrossRef]
102. Ren, W.J.; Ai, Z.H.; Jia, F.L.; Zhang, L.Z.; Fan, X.X.; Zou, Z.G. Low temperature preparation and visible light photocatalytic activity mesoporous carbon-doped crystalline $TiO_2$. *Appl. Catal. B Environ.* **2007**, *69*, 138–144. [CrossRef]
103. Neppolian, B.; Wang, Q.; Jung, H.; Choi, H. Ultrasonic-assisted sol-gel method of preparation of $TiO_2$ nano-particles: Characterization, properties and 4-chlorophenol removal application. *Ultrason. Sonochem.* **2008**, *15*, 649–658. [CrossRef]
104. Wang, X.K.; Wang, C.; Guo, W.L.; Wang, J.G. A novel single-step synthesis of N-doped $TiO_2$ via a sonochemical method. *Mater. Bull. Res.* **2011**, *46*, 2041–2044. [CrossRef]
105. Xu, H.; Zheng, Z.; Zhang, L.; Zhang, H.; Deng, F. Hierarchical chlorine-doped rutile $TiO_2$ spherical clusters of nanorods: Large-scale synthesis and high photocatalytic activity. *J. Solid State Chem.* **2008**, *181*, 2516–2522. [CrossRef]
106. Xu, H.; Zhang, L. Selective Nonaqueous Synthesis of C-Cl-Co-doped $TiO_2$ with Visible-Light Photocatalytic Activity. *J. Phys. Chem. C* **2010**, *114*, 11534–11541. [CrossRef]

107. Xiao, G.; Su, H.; Tan, T. Synthesis ofcore–shell bioaffinity chitosan–$TiO_2$ composite and its environmental applications. *J. Hazard. Mater.* **2015**, *283*, 888–896. [CrossRef]
108. Mazierski, P.; Nischk, M.; Golkowska, M.; Lisowski, W.; Gazda, M.; Winiarski, M.J.; Klimczuk, T.; Zaleska-Medynska, A. Photocatalytic activity of nitrogen doped $TiO_2$ nanotubes prepared by anodic oxidation: The effect of applied voltage, anodization time and amount of nitrogen dopant. *Appl. Catal. B Environ.* **2016**, *196*, 77–88. [CrossRef]
109. Arfanis, M.K.; Adamou, P.; Moutakas, N.G.; Theodoros, M.T.; Kontos, A.G.; Falaras, P. Photocatalytic degradation of salicylic acid and caffeine emerging contaminants using titania nanotubes. *Chem. Eng. J.* **2017**, *310*, 525–536. [CrossRef]
110. Vaiano, V.; Sacco, O.; Iervolino, G.; Sannino, D.; Ciambelli, P.; Liguori, R.; Bezzeccheri, E.; Rubino, A. Enhanced visible light photocatalytic activity by up conversion phosphors modified N-doped $TiO_2$. *Appl. Catal. B Environ.* **2015**, *176–177*, 594–600. [CrossRef]
111. Alrousan, D.M.A.; Polo-López, M.I.; Dunlop, P.S.M.; Fernández-Ibáñez, P.; Byrne, J.A. Solar photocatalytic disinfection of water with immobilised titanium dioxide in re-circulating flow CPC reactors. *Appl. Catal. B Environ.* **2012**, *128*, 126–134. [CrossRef]
112. Horovitz, I.; Avisar, D.; Baker, M.A.; Grilli, R.; Lozzi, L.; Camillo, D.D.; Mamane, H. Carbamazepine degradation using a N-doped $TiO_2$ coated photocatalytic membrane reactor: Influence of physical parameters. *J. Hazard. Mater.* **2016**, *310*, 98–107. [CrossRef]
113. Fabiyi, M.E.; Skelton, R.L. Photocatalytic mineralisation of methylene blue using buoyant $TiO_2$-coated polystyrene beads. *J. Photochem. Photobiol. A Chem.* **2000**, *132*, 121–128. [CrossRef]
114. Vaiano, V.; Sacco, O.; Sannino, D.; Ciambelli, P.; Longo, S.; Venditto, V.; Guerra, G. Ndoped $TiO_2$/s-PS aerogels for photocatalytic degradation of organic dyes in wastewater under visible light irradiation. *J. Chem. Technol. Biotechnol.* **2014**, *89*, 1175–1181. [CrossRef]
115. Singh, S.; Singh, P.K.; Mahalingam, H. An effective and low-cost $TiO_2$/polystyrene floating photocatalyst for environmental remediation. *Int. J. Environ. Res.* **2015**, *9*, 535–544.
116. Yuan, B.; Wang, Y.; Biang, H.; Shen, T.; Wu, Y.; Chen, Z. Nitrogen doped $TiO_2$ nanotube arrays with high photoelectrochemical activity for photocatalytic applications. *Appl. Surf. Sci.* **2013**, *280*, 523–529. [CrossRef]
117. Hou, X.; Wang, C.-W.; Zhu, W.-D.; Wang, X.-Q.; Li, Y.; Wang, J.; Chen, J.-B.; Gan, T.; Hu, H.-Y.; Zhou, F. Preparation of nitrogen-doped anatase $TiO_2$ nanoworm/nanotube hierarchical structures and its photocatalytic effect. *Solid State Sci.* **2014**, *29*, 27–33. [CrossRef]
118. Sun, L.; Cai, J.; Wu, Q.; Huang, P.; Su, Y.; Lin, C. N-doped $TiO_2$ nanotube array photoelectrode for visible-light-induced photoelectrochemical and photoelectrocatalytic activities. *Electrochim. Acta.* **2013**, *108*, 525–531. [CrossRef]
119. Kim, D.; Fujimoto, S.; Schmuki, P.; Tsuchiya, H. Nitrogen doped anodic $TiO_2$ nanotubes grown from nitrogen-containing Ti alloys. *Electrochem. Commun.* **2008**, *10*, 910–913. [CrossRef]
120. Hsu, H.C.; Shown, I.; Wei, H.Y.; Chang, Y.C.; Du, H.Y.; Lin, Y.G.; Tseng, C.A.; Wang, C.H.; Chen, L.C.; Lin, Y.C.; et al. Graphene oxide as a promising photocatalyst for $CO_2$ to methanol conversion. *Nanoscale* **2013**, *5*, 262–268. [CrossRef] [PubMed]
121. Sacco, O.; Vaiano, V.; Rizzo, L.; Sannino, D. Photocatalytic activity of a visible light active structured photocatalyst developed for municipal wastewater treatment. *J. Clean. Prod.* **2018**, *175*, 38–49. [CrossRef]
122. Huang, M.; Xu, C.; Wu, Z.; Huang, Y.; Lin, J.; Wu, J. Photocatalytic discolorization of methyl orange solution by Pt modified $TiO_2$ loaded on natural zeolite. *Dye Pigments* **2008**, *77*, 327–334. [CrossRef]
123. Gomes, J.; Quinta-Ferreira, M.E.; Costa, R.; Quinta-Ferreira, R.M.; Martins, R.C. Parabens degradation using catalytic ozonation over volcanic rocks Environ. *Sci. Pollut. Res.* **2018**, *25*, 7346–7357. [CrossRef]
124. Gomes, J.; Frasson, D.; Pereira, J.L.; Gonçalves, F.J.M.; Castro, L.M.; Quinta-Ferreira, R.M.; Martins, R.C. Ecotoxicity variation through parabens degradation by single and catalytic ozonation using volcanic rock. *Chem. Eng. J.* **2019**, *630*, 30–37. [CrossRef]
125. Fagan, R.; McCormack, D.E.; Dionysiou, D.D.; Pillai, S.C. A review of solar and visible light active $TiO_2$ photocatalysis for treating bacteria, cyanotoxins and contaminants of emerging concern. *Mater. Sci. Semicond. Process.* **2016**, *42*, 2–14. [CrossRef]
126. Ananpattarachai, J.; Seraphin, S.; Kajitvichyanukul, P. Formation of hydroxyl radicals and kinetic study of 2-chlorophenol photocatalytic oxidation using C-doped $TiO_2$, N-doped $TiO_2$, and C,N Co-doped $TiO_2$ under visible light. *Environ. Pollut.* **2016**, *23*, 3884–3896. [CrossRef]

127. Petala, A.; Frontistis, Z.; Antonopoulou, M.; Konstantinou, I.; Kondarides, D.I.; Mantzavinos, D. Kinetics of ethylparaben degradation by simulated solar radiation in the presence of N-doped $TiO_2$ catalysts. *Water Res.* **2015**, *81*, 157–166. [CrossRef]
128. Aba-Guevara, C.G.; Medina-Ramírez, I.E.; Hernández-Ramírez, A.; Jáuregui-Rincón, J.; Lozano-Álvarez, J.A.; Rodríguez-López, J.L. Comparison of two synthesis methods on the preparation of Fe, N-Co-doped $TiO_2$ materials for degradation of pharmaceutical compounds under visible light. *Ceram. Int.* **2017**, *43*, 5068–5079. [CrossRef]
129. Rajoriya, S.; Bargole, S.; George, S.; Saharan, V.K.; Gogate, P.R.; Pandit, A.B. Synthesis and characterization of samarium and nitrogen doped $TiO_2$ photocatalysts for photo-degradation of 4-acetamidophenol in combination with hydrodynamic and acoustic cavitation. *Sep. Purif. Technol.* **2019**, *209*, 254–269. [CrossRef]
130. Pedrosa, M.; Pastrana-Martínez, L.M.; Pereira, R.F.P.; Faria, J.L.; Figueiredo, J.L.; Silva, A.M.T. N/S-doped graphene derivatives and $TiO_2$ for catalytic ozonation and photocatalysis of water pollutants. *Chem. Eng. J.* **2018**, *348*, 888–897. [CrossRef]
131. Solís, R.R.; Rivas, F.J.; Gimeno, O.; Pérez-Bote, J.L. Photocatalytic ozonation of pyridine-based herbicides by N-doped titania. *J. Chem. Technol. Biotechnol.* **2015**, *91*, 1998–2008. [CrossRef]
132. Abramović, B.F.; Šojić, D.V.; Anderluh, V.B.; Abazović, N.D.; Čomor, M.I. Nitrogen-doped $TiO_2$ suspensions in photocatalytic degradation of mecoprop and (4-chloro-2-methylphenoxy)acetic acid herbicides using various light sources. *Desalination* **2009**, *244*, 293–302. [CrossRef]
133. Skoczko, I.; Piekutin, J. Photo-Fenton method usage to organic compounds degradation. *Desalin. Water Treat.* **2014**, *52*, 3837–3842. [CrossRef]
134. Martins, R.C.; Silva, A.M.T.; Castro-Silva, S.; Garção-Nunes, P.; Quinta-Ferreira, R.M. Adopting strategies to improve the efficiency of ozonation in the real-scale treatment of olive oil mill wastewaters. *Environ. Tecnhol.* **2010**, *31*, 1459–1469. [CrossRef]


© 2019 by the authors. Licensee MDPI, Basel, Switzerland. This article is an open access article distributed under the terms and conditions of the Creative Commons Attribution (CC BY) license (http://creativecommons.org/licenses/by/4.0/).